

L. Downer
B. R. Hester
H. F. Platts
Ra York
W. G. Kuster

RB-52

VIEWING STORAGE TUBES

GC CD ES JS PS
JWO JCN LES DR
RECEIVED
JUN 14 1956
O. R. TUBE ENGINEERING
NOTE FILE DISCUSS
ANS RETURN LOG



RADIO CORPORATION OF AMERICA
RCA LABORATORIES
INDUSTRY SERVICE LABORATORY

RADIO CORPORATION OF AMERICA
RCA LABORATORIES
INDUSTRY SERVICE LABORATORY

RB-52

Viewing Storage Tubes

This report is the property of the Radio Corporation of America and is loaned for confidential use with the understanding that it will not be published in any manner, in whole or in part. The statements and data included herein are based upon information and measurements which we believe accurate and reliable. No responsibility is assumed for the application or interpretation of such statements or data or for any infringement of patent or other rights of third parties which may result from the use of circuits, systems and processes described or referred to herein or in any previous reports or bulletins or in any written or oral discussions supplementary thereto.

Viewing Storage Tubes

This bulletin surveys the present state of the art on viewing storage tubes. Basic principles, theoretical operation, constructional techniques, and operating characteristics are given for several experimental tubes of this type.

Introduction

During the past few years nearly all of the published work on storage tubes has been on viewing tubes. These tubes are particularly useful in applications such as radar, facsimile transmission, oscilloscopy, and telemetering. Here the need exists for a bright visual display persisting for an extended period of time corresponding to information which has been written in a fraction of a second. In the past, one attempt to fulfill this need was the development of cathode-ray tubes with long persistence phosphors which permit the observation of a written picture up to several minutes, but only in a darkened room.¹ Another attempt was the darktrace storage tube² which employs the discoloration of a potassium chloride screen under electron bombardment and has a relatively long viewing duration. However, the contrast is too poor, the erasing time too long, and the life of the screen too short for many applications.

One solution is the combination of a signal-converter storage tube such as the Graphechon³ or the Metrechon⁴ with a conventional viewing cathode-ray tube. Such combinations are especially valuable where a stored picture is to be transmitted to several display points at the same time, since only one signal-converter storage tube is needed. However, for systems where only one display per receiver is necessary, a direct-view tube with storage is obviously preferable since less equipment is required. For applications where very high brightness is required, such as in daylight viewing or projection, the viewing storage tube is of particular advantage, because of its relatively low viewing-anode potential (less than 10 kv as compared to more than 50 kv in scanning projection tubes). For the same brightness, of course, the viewing currents of the storage tube are correspondingly higher.

Description of Typical Viewing Storage Tubes

Three types of direct-view storage tubes have been developed and described in the literature. These differ in the method of modulation of the viewing beam⁵, and may be classified as the emission control type, the bistable

landing velocity control type, and the transmission control type. The discussion following is concerned only with transmission control types of tubes since most recent work has been on this form of tube.^{6,7} For this method of control (Fig. 1) the storage target is constructed of a fine mesh metal screen coated on one side with an insulating material such as silica or magnesium fluoride. In operation the writing beam produces a pattern of charges on the insulating elements. The resulting potential variations locally control the transmission of a flooding viewing beam through the storage target. This beam is then accelerated toward a luminescent screen, producing a bright visual image of the stored charge pattern.

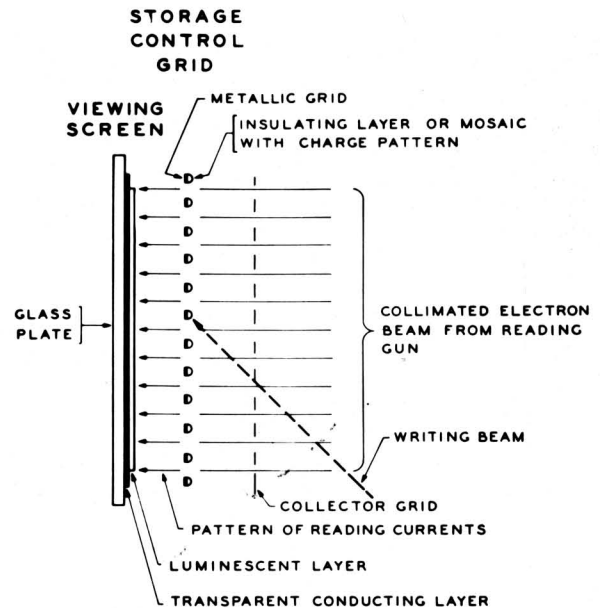


Fig. 1 - Arrangement for transmission control of flood beam in a viewing storage tube.

The potential pattern on the controlling storage grid may be produced by non-equilibrium writing, or bistable writing (with the viewing beam used as the holding beam). Not only secondary emission, but also bombardment-induced conductivity of the storage layer may shift its surface potential. Erasing is also performed by secondary

Viewing Storage Tubes

emission or bombardment-induced conductivity, using either the writing beam, the viewing beam, or a special erasing beam.

Fig. 2 shows the elements of a typical form of such a viewing storage tube. The writing and erasing beams are focused at the target and can be deflected. The viewing gun produces a flooding beam which covers the entire target. To insure that the viewing and erasing beam electrons arrive at the storage target with normal incidence a condenser lens is provided near the storage target, or the storage target is given a spherical shape.

The three closely-spaced electrodes at the front end of the tube, the collector grid, the storage grid, and the luminescent screen, comprise the image amplifier section where the picture patterns are written, stored and displayed, and erased. This group of electrodes, or target assembly, is referred to as an image amplifier because an increase in power takes place from the written to the viewed picture. Since the writing-beam current is at least 10 times less than the viewing-beam current, the power of the viewed picture is at least 10 times greater than that of the written picture for equal beam voltages. Because the stored pattern written in a fraction of a second may be observed for several minutes, the gain in work during such long storage is of the order of 10^6 .

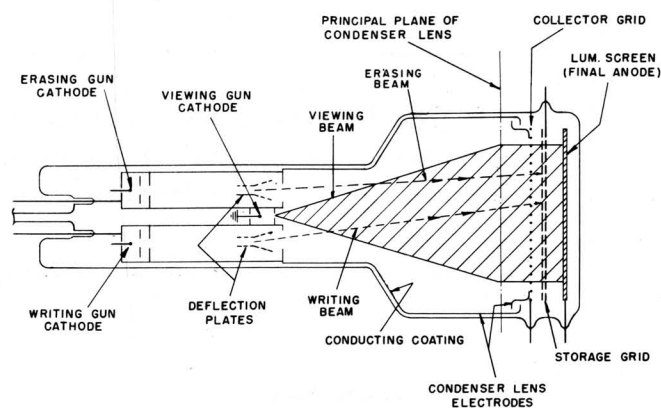


Fig. 2 -- Elements of a typical viewing storage tube.

A number of different types of viewing storage tubes have been built, both for direct viewing and for projection. For direct viewing, several versions (with about 4-inch target diameter) have been developed, particularly suitable for daylight operation in airplanes. One form of tube is suitable for storage of black-and-white (on-off) pictures.^{7,8,9} Another form is not restricted to black-and-white operation, but is also capable of producing half-tone pictures.^{6,8,9}

For larger displays, a 10-inch target diameter half-

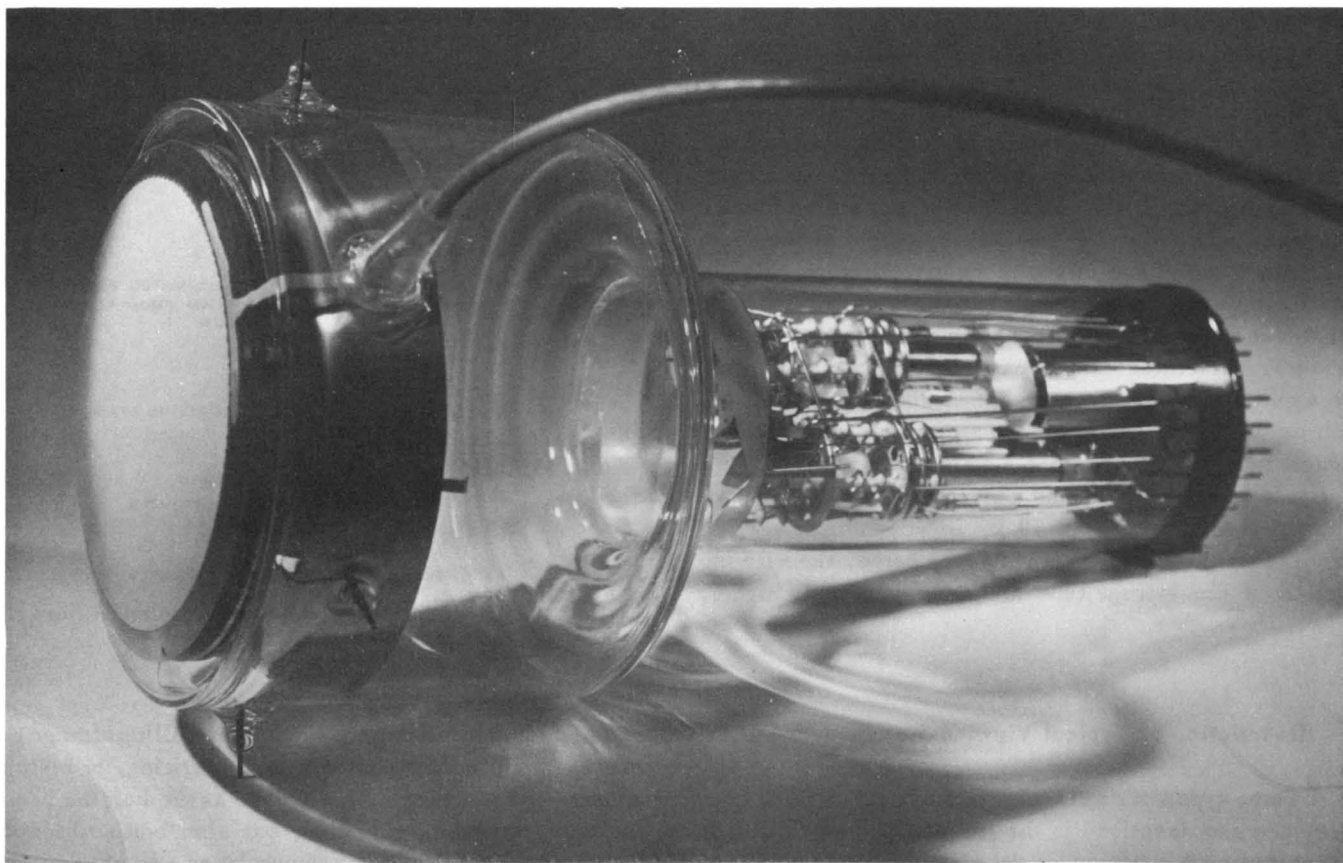


Fig. 3 -- Photograph of an experimental projection storage tube.

tone tube with a metal cone and wider viewing beam and deflection angles, has also been built.¹⁰ For very high brightness several types of tubes have been designed. One of 2½-inch screen diameter¹¹ and one of 4-inch screen diameter, both with curved faceplates, are suitable for use in projection systems. In the 4-inch tube, non-uniformity in the viewing-beam background (due to condenser lens aberrations) was avoided by using a curved storage grid and an approximately concentric collector grid. These reduce the required refractive power of the condenser lens, thus largely eliminating the spherical aberrations.

In tubes with flat grids, selective erasure of individual target points is difficult unless a complex double condenser lens is used. Such erasure is made easier, however, by the use of curved grids in the image amplifier section.

Fig. 3 shows a photograph of an experimental projection storage tube which may also be used for very bright direct-view applications. The ion pump and the writing and erasing guns, which are both parallel to the tube axis, can be seen in the tube neck. The viewing gun is quite short and is located coaxially between the writing and erasing guns.

Electron Transmission Characteristics of The Image Amplifier System

Before discussing the writing and erasing processes, the image-amplifier characteristics will be discussed. These determine the range of potentials on the storage grid necessary for modulating the viewing beam. In actual operation the insulating surface of the storage grid has potentials different from the supporting mesh. However, since differences of the order of only 10 volts or less exist with respect to the supporting mesh (which is slightly positive with respect to the viewing gun cathode), to a first approximation the characteristics of the storage target with no insulating material can be used as a model for analysis of the operation. In general, the image-amplifier section, consisting of the collector grid, the storage grid, and the anode (supporting the phosphor screen), together with the viewing-gun cathode comprise a space charge grid tetrode.¹² The characteristics of such a system as measured by Rothe and Kleen¹³ are given by Fig. 4. These authors found that the shape of these characteristics is quite different at high and low current densities, depending on whether electron optic or space-charge conditions prevail near the control grid. In addition, a typical shift of the cut-off voltage takes place within the electron optic region for different maximum anode currents. Equations for characteristics of this kind

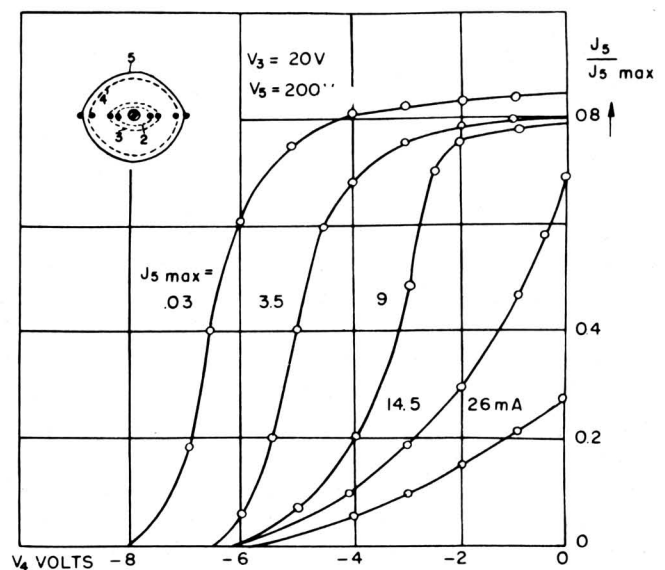


Fig. 4 - Characteristics of a space-charge grid tetrode as a function of anode current (Rothe-Kleen).

of tetrode exist for the space-charge case, showing the well-known $V^{3/2}$ rise. For the electron optic range, useful equations have been developed only for the case where the field gradients on both sides of the control grid are equal.¹³ For the storage tube, however, the gradient on the collector grid side should be low to minimize the spherical aberration of the condenser lens. Also the gradient on the luminescent screen side must be high to get adequate brightness and resolution and to shift the control characteristic towards more negative V_2 potentials. Because the anode current density in the storage tube is low (of the order of $10 \mu\text{amp}/\text{cm}^2$), and the field gradient near the control grid holes is high (which presumably causes an "electron optic" current distribution), characteristics of the type shown in the left part of Fig. 4 are found.

In an actual tube the characteristics may be measured with either current or phosphor screen brightness as the dependent variable (using a phosphor with a light output proportional to the incident current). The total current is only an average of the individual characteristics for different sections of the target. By using a photomultiplier which is arranged to "see" only a very small area of the luminescent screen, the characteristics of a particular area may be obtained.

Measurements of the characteristics of tubes with bare grids are easily made by ordinary methods. However, for tubes with storage layers, the viewing duration, due to ion bombardment of the average layer, is too short for convenient measurements. A more rapid, automatic method for taking these data consists of applying to the grid a linear sawtooth of voltage from a motor-driven potentiometer and plotting the brightness or current with an

electromagnetic recording oscillograph. A sawtooth period of 10 seconds was found to be a satisfactory compromise between phosphor decay and limited viewing duration.

In recording such characteristics the insulator surface is first charged uniformly with respect to its backplate by secondary emission. The storage mesh is then switched negative and the sawtooth voltage started. At the positive excursion of the sawtooth the insulator surface is charged to viewing-cathode surface potential which is taken as zero insulator potential. During the second sawtooth a recording is made. By shifting the mesh bias positive in steps, a family of characteristics can be recorded. Actual image amplifier characteristics for different mesh grids without storage layers are shown in Fig. 5. As expected, there is a close similarity to the low current density curves of Rothe and Kleen. However, there is a substantial shift towards positive grid potentials due to the high amplification factor (1,000 to 10,000) of the finer mesh in spite of the 20 times larger gradient.

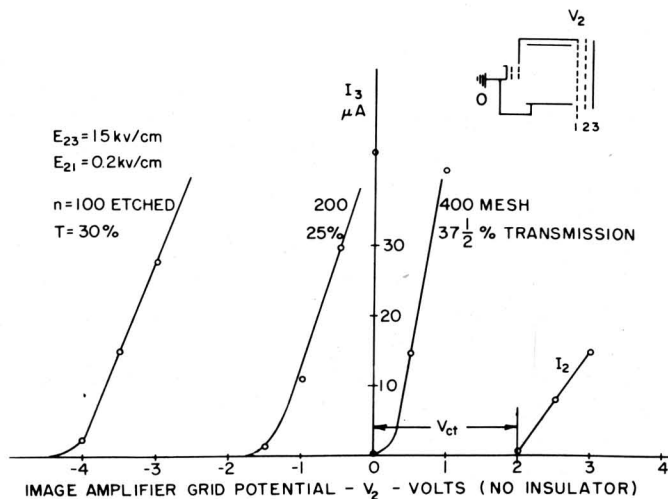


Fig. 5 - Viewing current characteristics for bare control grids with different mesh.

As can be seen from the grid current curve, I_2 , storage is possible up to an indicated voltage of +2 volts because the landing current starts only at this high value. This voltage is the sum of contact potential and cathode interface voltage drop. One reason for this high value is that the clean target grid metal is less likely to be contaminated by a barium layer as occurs frequently in amplifier tubes. Also, since the viewing-cathode current is nearly independent of the target grid potential, the cathode interface voltage drop remains high even at low viewing-screen currents.

Control grids of 400 mesh and even finer are, therefore, suitable for image amplifiers, if the anode gradient is sufficiently high. However, such fine grids may not be necessary from the standpoint of resolution since a 250-

mesh grid provides adequate resolution for displaying television pictures on a 4-inch viewing screen. Extrapolating to a 12-inch viewing screen, for example, indicates that an 80-mesh grid would suffice for this purpose. The choice of type of grid mesh and of hole spacing may depend on background disturbance, which is separately discussed.

Fig. 6 shows the static characteristics recorded for a 200-mesh grid where the storage surface and the metallic mesh supporting it are at the same potential. These characteristics were measured as described, making the positive excursion of the sawtooth voltage equal to the viewing-cathode potential. The curves are plotted only to 30 μ amp so that the region near cutoff may be shown in more detail. As in the bare grid case, the characteristics show a typical shift to the left with rising anode gradient. From this shift the amplification factor may be determined.

One might assume that the dynamic characteristics of the image amplifier systems are identical with the grid characteristics shown in Fig. 6 because only small voltages are necessary to control the anode current. Actually, this is not the case because of the action of the gradient across the storage layer. Since the distance between the storage layer surface and metal mesh (backplate) is only a few microns, gradients of 10^5 volts/cm arise across the storage layer. For the usual case with the mesh positive with respect to the storage layer surface, the action of this gradient near the grid holes shifts the characteristic towards negative V_2 potentials, as if the anode potential had been raised.

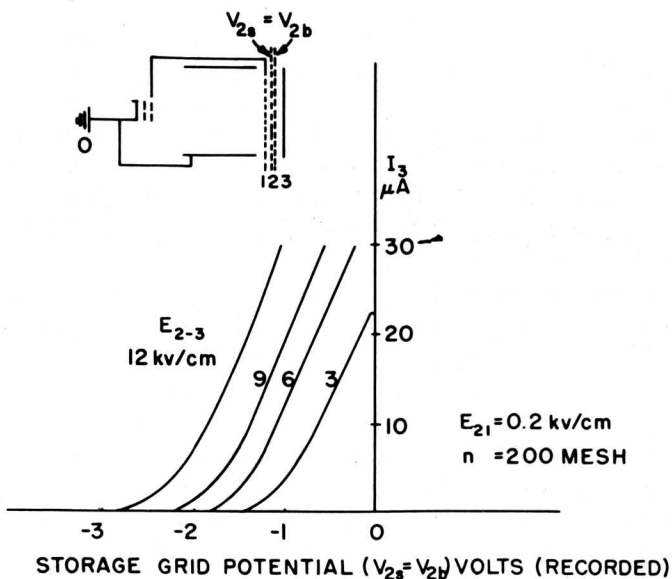


Fig. 6 - Viewing current characteristics for a coated control grid with no gradient across the insulator.

In Fig. 7 a family of such static characteristics is shown in which the potential difference across the storage layer ($V_{2b} - V_{2s}$) is kept constant while the storage sur-

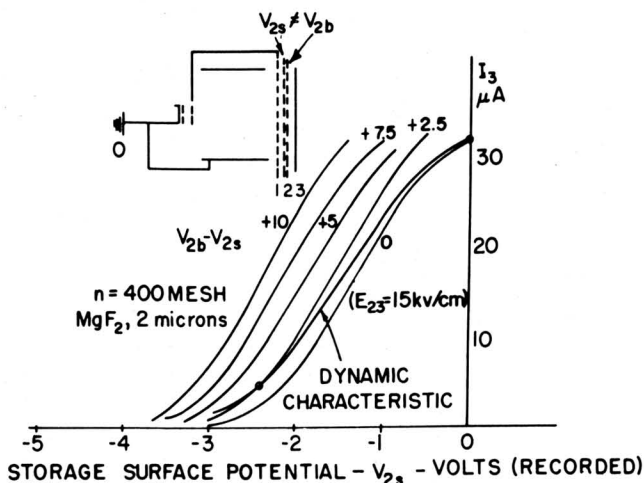


Fig. 7 - Viewing current characteristics for a coated control grid with different gradients across the insulator.

face potential, V_{2s} , is changed. Comparing Fig. 7 with Fig. 6 it can be seen that 10 volts change in the surface-to-mesh potential shifts the characteristics by an amount corresponding to an increase of anode voltage, V_3 , of about 100 percent.

The dynamic characteristic, therefore, must have a smaller slope than the static characteristic. The maximum dynamic anode current, I_{3max} , is the intercept of the static characteristic corresponding to the backplate bias, with the $V_{2s} = 0$ ordinate. Lower I_3 values belong to other static characteristics with successively higher gradients.

As an example, the dynamic characteristic for $V_{2b} = 0$ is given by the following conditions: $V_{2s} = 0$, $V_{2b} - V_{2s} = 0$; $V_{2s} = -1$, $V_{2b} - V_{2s} = +1$; $V_{2s} = -2$, $V_{2b} - V_{2s} = +2$; $V_{2s} = -3$, $V_{2b} - V_{2s} = +3$; etc.

The smaller slope of the dynamic characteristics is advantageous with respect to the signal-to-disturbance ratio. Furthermore, the use of a higher potential difference, $V_{2b} - V_{2s}$, than actually needed for grid control, presents a new possibility of shifting the dynamic characteristic to more negative surface potentials. For a fine mesh grid this might prevent electron landing, and permit using smaller anode gradients. For the grids investigated, the shape of the dynamic characteristics changes only slightly with increasing $V_{2b} - V_{2s}$.

Electron Optical Requirements for The Image Amplifier System

Electron Lens Raster Systems (Storage Grid Resolution^{6,14})

For imaging the charge picture (written on the storage layer) on the luminescent anode screen with satisfactory resolution, an electron lens raster is employed. This is provided by the storage grid holes, each of which focuses that portion of the viewing-beam current passing through it into a separate beam and to a single spot on the viewing screen. Proper focusing of the individual spots is dependent on the geometry and the potentials of the image-amplifier electrodes.

In Fig. 8 is shown schematically a number of these miniature lenses, and the elementary beams produced by them. To avoid loss in resolution due to overlapping of the elementary beams, their diameter at the luminescent screen should not exceed the hole distance of the storage grid. The condition when the spots are tangent to each other at the screen is defined as the "tangent dot condition".

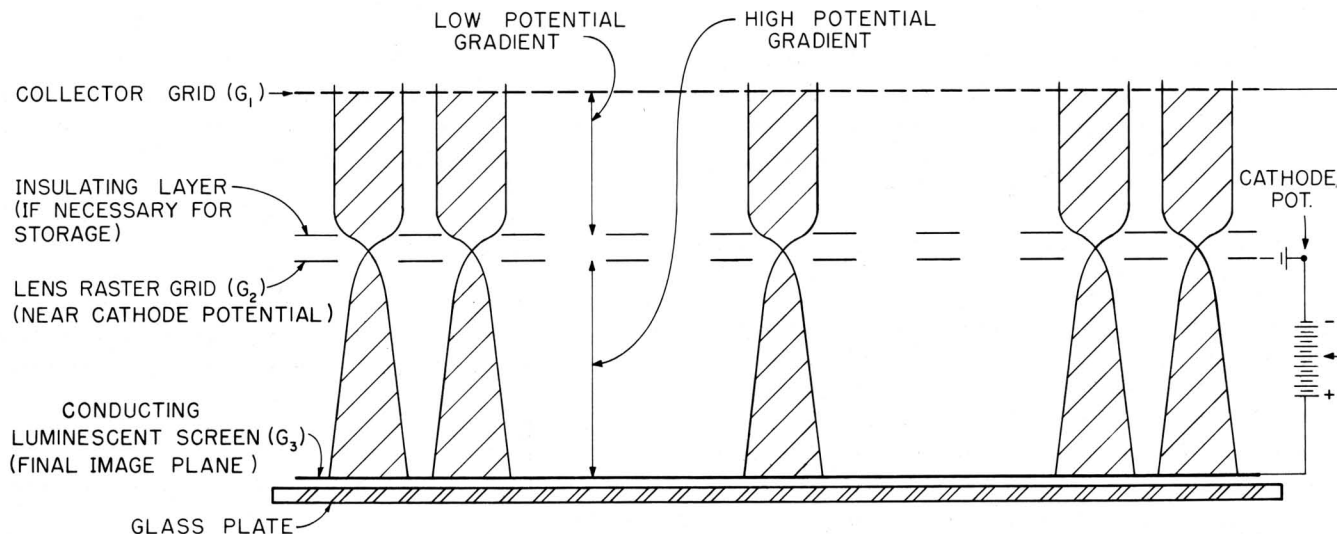


Fig. 8 - Beam focusing by electron lens raster system.

In Fig. 8 the mesh support and the storage layer are assumed to be at the same potential, $V_2 = 0$. These conditions correspond to highlight conditions in the stored picture. At lower light levels, corresponding to negative potentials on the storage layer, the dots become smaller and more separated. Because the resolution does not deteriorate in this range, the computations and experiments for the dot focusing can be based on the case of a bare storage grid near cathode potential.

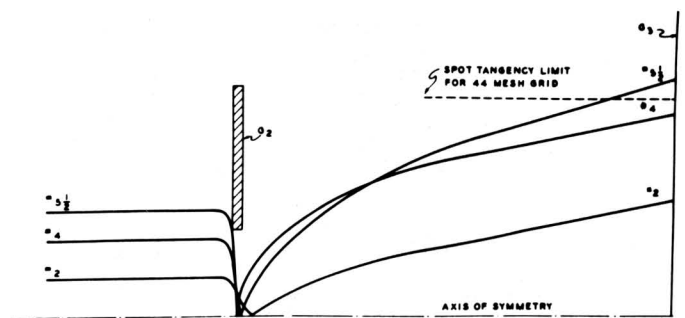
Figs. 9a, b, and c show the electron paths* of three such elementary beams for a bare control grid with cylindrical, conical, and biconical holes. Due to the necessarily large difference of the electrical gradients on both sides of the storage grid (the gradient ratio here was chosen ≈ 30) all electron paths cross the optical axis within a distance as close as 0.2 to 1 hole diameter from the surface (gun side) of the storage grid. As a result, strong spherical aberrations occur, which lead to a typical non-uniform beam current distribution on the luminescent screen (Fig. 10) which may be observed through a microscope (or directly in an enlarged electron optic model) as a bright dot with a bright concentric ring superimposed on a moderately bright uniform background¹⁵.

It should also be noted that for the bare grid at cathode potential the cylindrical holes produce a smaller elementary spot at the luminescent screen than the conical or biconical ones which, on the other hand, exhibit a higher ratio of electron transparency to light transparency than the cylindrical ones (beams 2 to $5\frac{1}{2}$ in Fig. 9a as compared to beams 2 to 7 in Fig. 9b). However, this difference in spot size becomes smaller if a negative storage grid potential is applied in the conical hole case which produces the same electron current to the anode as the cylindrical holes at zero potential. For picture uniformity it is thus necessary that not only the size of the holes, but also their profile (i.e., conical or cylindrical, for example) be maintained uniform.

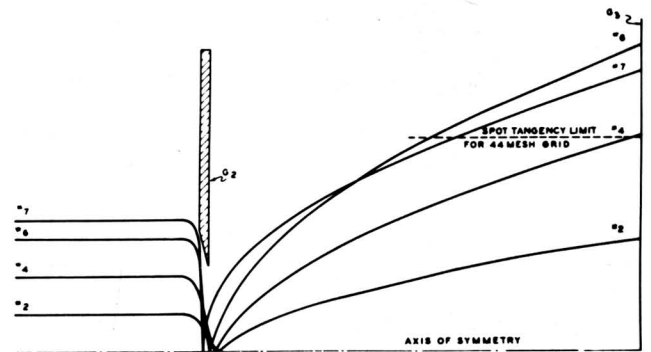
It can be seen from Figs. 9a and 10 that for the gradients and electrode dimensions chosen, the dots of the elementary beams are tangent (or overlapping slightly). In accordance with the electron optic laws of similarity, this "tangent dot condition" should also occur:

- (a) For other electron lens raster systems, the dimensions of which are magnified or demagnified

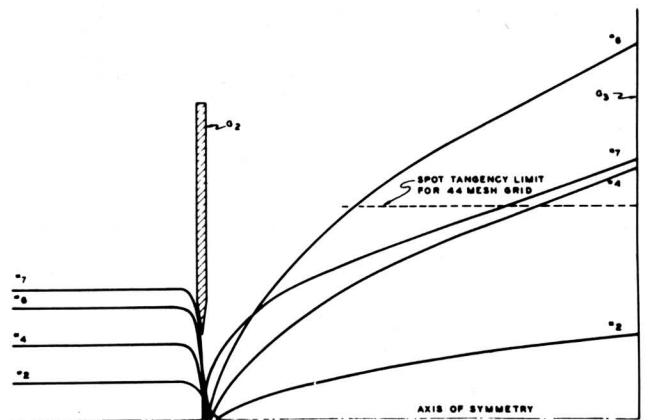
*Determined from the field measured in a resistance network model and with the graphical method (Snell's Law) by H. Hook and W. Kosonocky. For the electrode configuration in Fig. 9a some of the paths have also been calculated with a computer. Their crossover distances from the storage grid differed by less than ± 3 percent from the ones found with the graphical method.



(a) cylindrical hole of bare control grid



(b) conical hole



(c) bi-conical hole

Fig. 9 - Electron paths of an elementary beam in an electron lens raster system (ratio of hole radius to grid-phosphor distance increased by a factor of 8)

in geometrical proportion, the voltages being the same, or

- (b) For identical lens raster systems, if the electrode voltages with respect to viewing-gun cathode are increased or decreased proportionately.

As a result of (b):

$$V_1 : V_2 : V_3 = K_1 : K_2 : 1, \text{ where } K_1 \text{ and } K_2 \text{ are constants.}$$

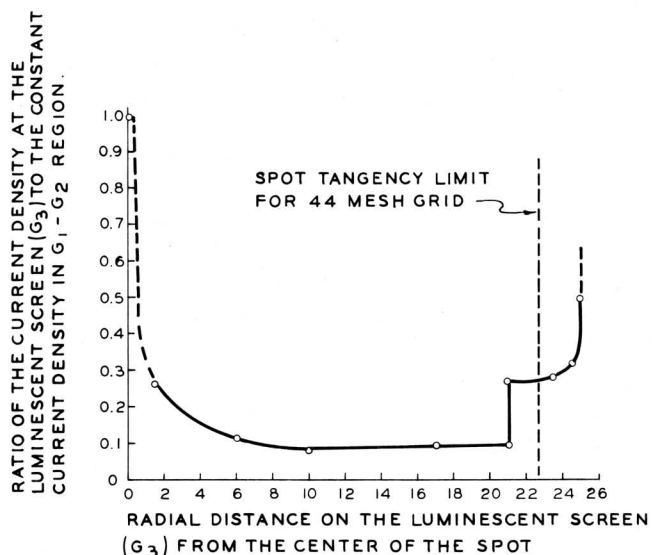


Fig. 10 - Current density distribution of an elementary beam at the phosphor for a cylindrical hole control grid.

Fig. 11 gives the tangent dot characteristics* for a control grid with 100 etched round holes per linear inch and 39 percent light transparency for corresponding V_2 and V_3 voltages. It has been found experimentally that tangent dot conditions can be obtained for different field ratios on both sides of the storage grid. By the law of similarity mentioned above, tangent dot conditions would be expected along straight lines going through the origin. The measured points are actually found to lie on straight lines but instead of passing through the origin, such as

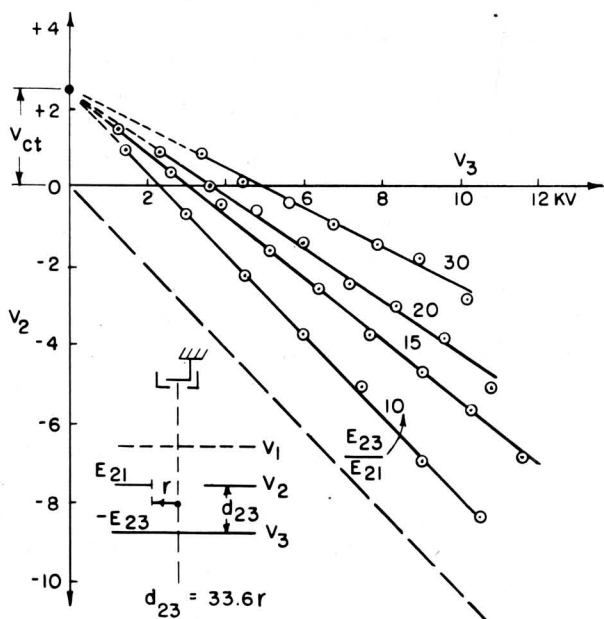


Fig. 11 - Tangent dot characteristics for a bare control grid (etched, 100 round holes per linear inch, 39 percent light transparency).

*For a detailed explanation, see Ref. 6.

the dotted line, they intersect the V_2 axis at approximately 2.5 volts. The reasons for this seems to be: (a) the contact potential between storage grid and viewing-beam cathode, and (b) the voltage drop across the oxide coating of the viewing-beam cathode.

Fig. 12 shows similar experimental characteristics for a control grid with 200 square holes per linear inch and 25 percent light transparency. It can be concluded that with electroformed grids, in spite of the astigmatism to be expected from the square holes, it is possible to separate 200 elementary beams per linear inch with final anode potentials of 10 kv, suitable for bright (daylight viewed) pictures at the phosphor screen.

The accuracy of the above method of determining the dot conditions with a microscope can be estimated by the deviations of the points from the straight lines. Because of the greater lens errors with square holes (Fig. 12) the accuracy is less for these holes than for the case of round holes (Fig. 13). As a result of the relatively small space charge density in the elementary beams such tangent dot diagrams are independent within wide limits of the flooding beam current arriving at the target.

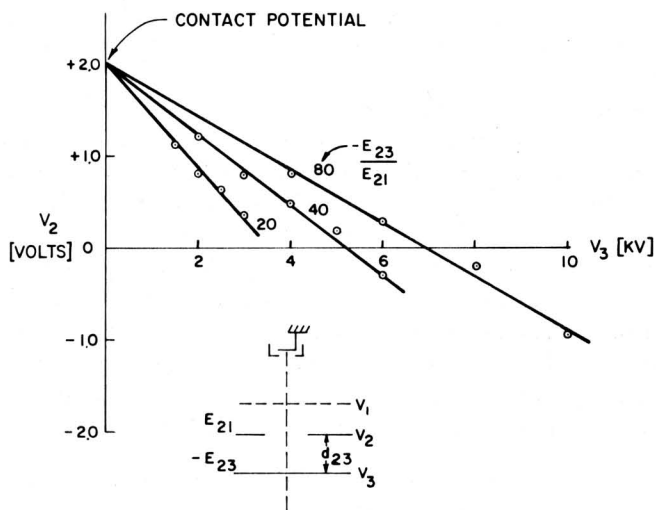


Fig. 12 - Tangent dot characteristics for a bare control grid (electroformed, 200 square holes per linear inch, 25 percent light transparency).

In general, the viewing-current characteristic is determined by the ratio of the field strengths on both sides of the storage target¹⁶. The question arises as to what part of the characteristic is useful within the limitation of the tangent dot conditions. In Fig. 13 are shown, for various field strength ratios, experimentally determined (by varying the collector voltage, V_1) conditions for cut-off, tangent dot, and saturation for an etched storage grid with circular holes and 10 percent light transmission. As can be seen, the highest gradient ratio gives a tangent

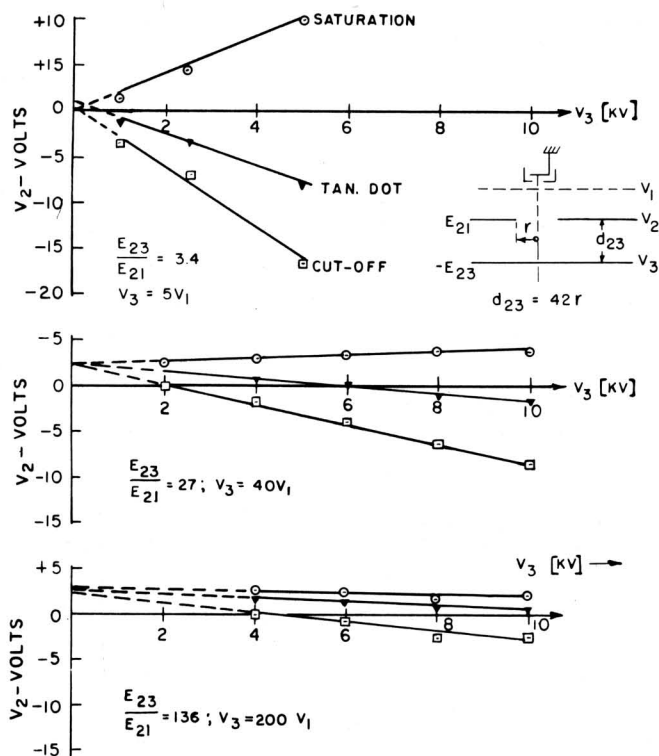


Fig. 13 - Tangent dot saturation, and cut-off conditions for a bare control grid (etched, 44 round holes per linear inch).

dot line which is closest to the saturation line*. In addition, the saturation currents for a given anode voltage were found to be correspondingly higher for the higher gradient ratios. For a given current at the phosphor screen, the high gradient ratio (low V_1 voltage) requires the least flooding-beam current arriving at the storage grid, thus permitting maximum viewing duration because of the correspondingly smaller ion currents. For example, an increase of phosphor-screen to flooding-beam current ratio of 3 was measured for an increase of gradient ratio from 3.4 to 136 with the system of Fig. 13.

Employing the electron optic law of geometric similarity, one finds reasonable agreement for the tangent dot characteristics measured for comparable systems such as in Figs. 11 and 13. In Fig. 11, for example, one has to insert a virtual anode at a distance of $0.3 (100/44) = 0.68$ cm, if its characteristics are applied to an equivalent system with a 44 hole per inch control grid as shown in Fig. 13.

In general, higher ratios of phosphor-screen to flooding-beam current should also be expected with in-

creasing light transparency of the storage grid. Actually, this ratio was found to be 0.1 for the system of Fig. 13 (10 percent transparency) and 0.3 for the system of Fig. 12 (25 percent transparency).

Concentric nonuniformity patterns of the viewing beam (due to spherical aberrations of the condenser lens) progressively disappear as the collector voltage decreases or the final anode voltage increases (this effect seems to be associated with a displacement of the saddle-point plane of the lens raster towards the collector grid). Therefore, for a fixed maximum anode voltage, the high gradient ratio desirable, as mentioned above, also improves the uniformity of the viewed picture by reducing the shading.

Flood Beam Condenser Systems

For ideal uniformity of the picture, the flooding electrons must arrive normal to the surface of the storage grid; thus, a collimating condenser lens is needed. With a flat storage grid and a point source of the flood beam, a single condenser lens close to the collector grid appears to be the most practical arrangement for a large ratio of picture diameter to tube diameter (Fig. 14a). One electrode of this lens may be formed by the collector grid, the other by a conducting wall coating (at viewing gun anode potential). In such an arrangement, even after careful collimation, concentric nonuniformities remain which are mostly caused by spherical aberration of the condenser lens (as in Fig. 15a); they disappear, however, as the aperture of the viewing beam is decreased (Fig. 15b). Similar but asymmetric nonuniformities have been found due to magnetic poles in the storage or collector grid frames (Fig. 15c). As mentioned above, both types of nonuniformity can be reduced by increasing the voltage gradient on the phosphor side. Thus, for a uniform picture background, a low collector grid voltage (< 100 volts) is desirable for flat image amplifiers. On the other hand, in order to prevent positive ions from landing on the storage grid, the collector grid must be more positive than any electrode between it and the viewing or erasing beam cathodes. Also, a higher collector grid voltage (> 100 volts) is desirable to obtain optimum gun voltage for a well-focused erasing beam. As a result, there must be a compromise between either concentric nonuniform background or poor erasing beam resolution for a viewing storage tube with a flat storage target and a single condenser lens. This system, however, may frequently be tolerated if overall (flooding) erasure with the viewing beam is used.

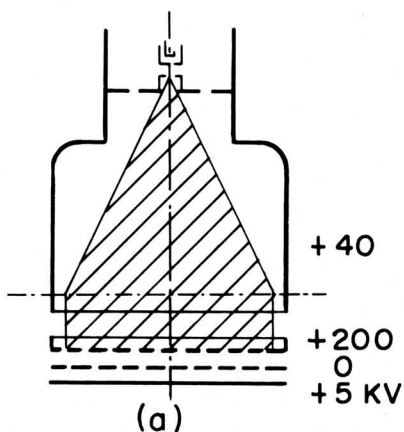
A way to make possible reasonably selective erasure in a viewing storage tube with a flat image amplifier is to introduce a double condenser lens (Fig. 14b). This provides three advantages:

*As indicated, V_1 was set at different proportions to V_3 in the lines of Figs. 11, 12, and 13. As shown for each constant value of V_3 the cutoff voltage of the viewing current characteristic decreases with high gradient ratios. However, if V_1 is kept constant, the cutoff voltage increases with higher gradient ratios, see p. 1498, Ref. 9.

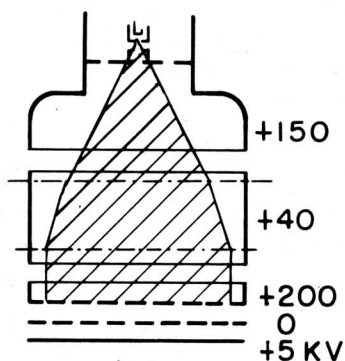
- (2) More parallel incidence of the flood beam.
- (3) Less space charge defocusing of the erasing beam in the condenser lens region.

However, although selective erasing is possible with the double condenser lens, present designs of such low voltage erasing guns with a well-focused beam provide only sufficient current density for slow writing speeds. To a certain degree, therefore, the same compromise exists between concentric background patterns and slow or poorly focused selective erasing for the double condenser lens.

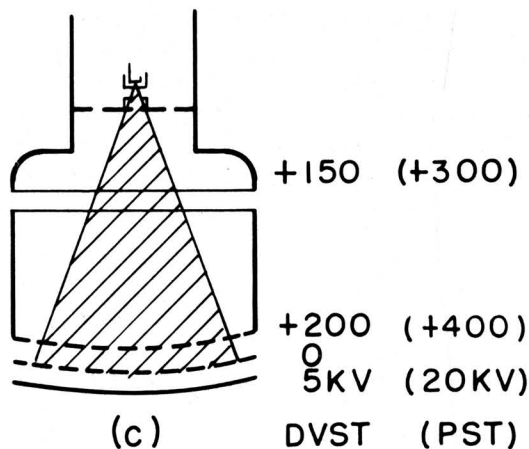
This compromise is much less severe for spherical image amplifier systems (Fig. 14c). In this case, normal



(a)
SINGLE LENS FLAT
GRIDS



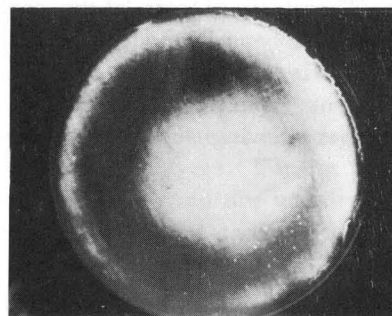
(b)
DOUBLE LENS FLAT
GRIDS



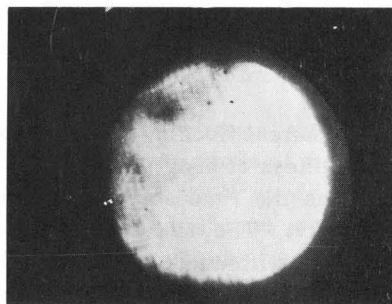
(c)
SINGLE LENS CURVED
GRIDS

Fig. 14 - Flood beam condenser systems.

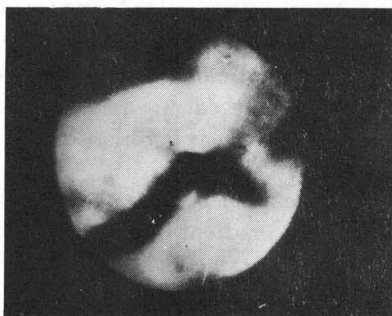
- (1) The erasing (and viewing) gun anode voltage may be as much as 70 percent of the collector voltage instead of less than 20 percent for the single condenser lens.



(a) 10 inch diameter picture with brightness adjusted to emphasize spherical aberration



(b) 8 inch diameter picture showing decrease in spherical aberration from (a)



(c) magnetic disturbance (4 inch tube)

Fig. 15 - Non-uniformity due to lack of incidence of viewing beam at storage grid.

incidence can be obtained by simply placing the viewing beam crossover near the center of curvature of the storage grid. Thus, only a weak condenser lens is needed for small corrections of the angle of incidence, and for repelling positive ions which would otherwise land at the storage target. Because of its position in a region of small flood beam diameter, such a weak condenser lens has a very small spherical aberration. Thus it permits a higher collector voltage (up to 500 volts) and also higher voltages for the anodes in the viewing and erasing guns that are essential for high brightness (with conventional guns) and high current density of the erasing beam spot.

Since the viewing beam is not collimated, its diameter at the lens can be considerably smaller than the lens diameter. Therefore, placing of the condenser lens nearer to the viewing beam cathode is possible without increasing the viewing beam angle. By using a smaller portion of this lens, spherical aberration is further reduced and a larger viewing screen may be used for the same bulb size.

Brightness, Resolution, and Writing Speed

The maximum brightness of the viewed picture is determined by the current in the viewing beam and the potential of the final anode or phosphor screen. For practical purposes, viewing beam currents of about 1 ma are readily obtainable with conventional cathode-ray tube gun structures.

With such a current flooding a 4-inch-diameter storage target, a brightness of about 300 foot lamberts is obtained with 5 kv on the final anode and about 5000 foot lamberts with 15 kv. The more than proportionate increase of brightness with anode voltage is due to better penetration of the aluminum backing and the phosphor layer. In principle, greater brightness can be obtained by higher anode voltages. However, breakdown due to the high gradients between the electrodes limits the voltage which can be used. In addition, phosphor screens prepared by the techniques used in manufacturing television tubes, where practically no gradient is present at the phosphor surface, are damaged by the phosphor pulling apart in this high gradient application.

Satisfactory phosphor screens can be produced suitable for withstanding gradients of the order of 30 kv/cm by settling a very fine-grained phosphor and rinsing it in a silicate solution. After baking, the phosphor is firmly bound to the glass support. (Such a phosphor screen has an "egg shell" appearance and can be rubbed lightly with a finger tip without damage). Then a very thin collodion film is deposited which permits phosphor par-

ticles to protrude through and bond directly to the aluminum layer, which is then evaporated on the collodion. Spark-overs produce a shiny spot on the aluminum, but no damage to the phosphor screen.

Tubes with 4-inch targets may have storage-screen-to-anode spacings of 1/8 to 1/4 inch. In general, the use of tubes with larger target diameters (10 inches for example) permit proportionately greater spacing between the phosphor screen and storage target so that correspondingly higher phosphor voltages may be employed.

Additional screen brightness can also be obtained with higher viewing gun currents. Although considerable increase is possible beyond the 1 ma level, the maximum size of the gun cross-over which can be tolerated without affecting the normal incidence of the viewing beam at the storage target has not been determined.

With present storage tubes, the average power dissipated at the storage screen is below that of high-voltage projection tubes so that higher brightness can be expected from future storage tubes without exceeding the power handling capability of the phosphor screen.

One of the primary advantages of the viewing storage tube is the relatively low beam currents required for writing (approximately 10 to 100 microamperes). Although only about 2 kv anode potential is used for these guns, the low beam current permits a resolution of 500 lines on a 4-inch target. In actual tubes, the resolution of the viewed picture may be limited by the hole spacing and geometry of the image amplifier section.

The maximum writing speed, v_{\max} (spot diameters per second), for a storage layer with a thickness, d_s (inches), can be calculated from the secondary writing current, i_s (amps), the control potential difference, V_s (volts), at the storage surface (measured between the lowest half-tone and the black level) and the storage element capacity, C_e (farads).

$$\text{Since } \frac{i_s t}{V_s} = C_e$$

where t is the time for charging one storage element to voltage, V_s ,

$$\frac{1}{t} = v_{\max} = \frac{i_s}{V_s C_e} \quad (\text{spots per second}) \quad (1)$$

In the above,

$$i_s = i_{pr} (1-a)(\delta-1)$$

where i_{pr} is the primary writing beam current, a is the

fraction of i_{pr} absorbed by the collector grid, δ is the secondary emission factor of the storage layer; and

$$C_e = \frac{(k)(A)(10^{-12})}{(4.45)(d_s)}$$

where A is the writing spot area, k is the dielectric constant, d_s is the storage layer thickness.

For $k = 5$ (MgF_2 layer), spot diameter 0.03 inch. (200 lines on 400 mesh storage grid), and $d_s = 16 \times 10^{-4}$ inches (4 microns), $C_e = 5 \times 10^{-12}$ farads. For $i_{pr} = 100 \times 10^{-6}$ amp, $a = 0.5$, $\delta = 5$ ($V_{wk} = 3000$ volts), $i_s = (100 \times 10^{-6})(0.5)(5-1) = 2 \times 10^{-4}$ amp and using a value of $V_s = 0.3$ volts (from characteristic for 400 mesh per inch storage grid), Eq. (1) gives the maximum writing speed:

$$v_{max} = \frac{(2 \times 10^{-4})}{(0.3) \times (5 \times 10^{-12})} = 1.33 \times 10^8 \text{ (spots per second)}$$

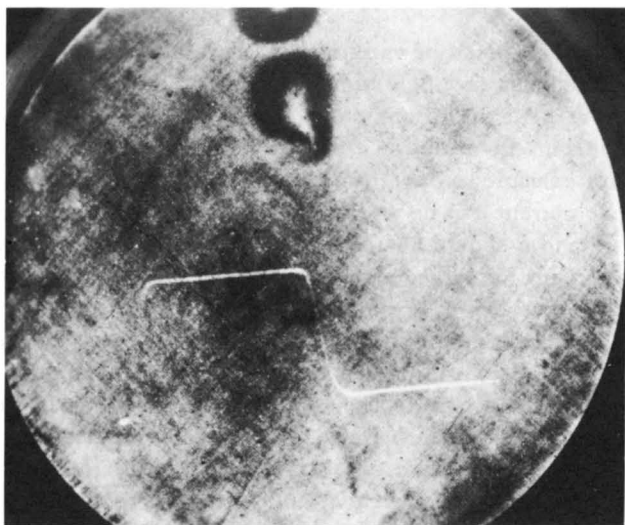


Fig. 16 - Photograph of stored single transient of one microsecond duration (0.1 microsecond rise time).

For a 4-inch target, this corresponds to about 5 cm per microsecond, or 50 km/sec. In Fig. 16 a single transient is shown recorded at about this speed on a 4-inch direct view storage tube, with values of C_e , d_s , i_s , and V_s as indicated above.

Writing speeds at least one order of magnitude higher may be obtained by increasing the thickness, d_s , of the storage layer.

Elimination of Picture Disturbances Originating in The Image Amplifier Section

For storage grids of viewing tubes, small hole spacing, accurate spacing between grid and anode, and

sufficient transparency are generally desirable, as well as high resistivity and proper secondary emission characteristics of the insulator. A high degree of uniformity of these factors over the target area is very essential. In the following, considerations and testing methods are discussed which have been developed for the purpose of improving this uniformity.

Fine Mesh Metal Grids

Theoretical requirements for uniformity. For minimizing the lens action of the collector grid, it should have a hole spacing at least as small as the smallest picture element. In addition, it should also be uniform enough over picture areas to avoid the superposition of a background shadow pattern on the picture. (It should also have a high transparency to minimize absorption of the flood beam).

Even stricter requirements hold for metal grids used as a base for storage layers. For the purpose of transmission control, such grids are usually operated at potentials near reading beam cathode potential. From the design of variable- μ amplifier tubes it is known that under such conditions variations in amplification factor, μ , (for example, variable grid wire spacing) will cause a decrease of the slope of the anode current characteristic with increasing bias. This decrease is understood to be a superposition of a number of elementary characteristics from different grid areas. These local variations in μ are accompanied by simultaneous variations of anode current in different grid areas for the same grid potential.

In image amplifier systems, the same effect occurs with regard to random variations of the amplification factor. The resultant variations in anode current distribution cannot be tolerated for half-tone reproduction by image amplifier systems, because they add a nonuniform background to the pictures to be amplified. However, black-and-white (on-off) pictures can be obtained with such nonuniform amplifier systems, by charging the storage grid either to a high negative potential so that all areas are cut off or to a very low potential where a relatively high viewing current is produced and where the percent variation in viewing current due to variations in μ are small.

An estimate as to the degree of uniformity required for metal meshes of half-tone image amplifiers may be derived from the equation for the space charge anode-current characteristic which assumes the existence of a virtual cathode between storage and accelerator (collector) grid*.

*This condition has not yet been realized in present day storage tubes; it can be expected to prevail at current densities of the order of 1 ma/cm² and higher, and is recognizable by the observed viewing beam characteristic where the slope increases with increasing current

If we suppose the storage surface to be at the same potential, V_3 , as the supporting mesh, it is identical with the equation for the space charge grid tetrode¹⁷:

$$J_4 = \frac{c}{d^2} (V_{3\text{eff}})^{3/2} = \frac{c}{d^2} \left[\frac{V_3 + \frac{V_4}{\mu_{43}}}{1 + \frac{1}{\mu_{43}} \left(1 + \frac{4}{3} \frac{d_{43}}{d}\right)} \right]^{3/2} \quad (1)$$

where c is a constant, d the distance of the virtual cathode from the storage grid (which increases slightly with J_4), V_3 the control grid potential, V_4 the anode potential, μ_{43} the amplification factor, and d_{43} the distance between anode and storage grid. In this formula, the anode current, J_4 , appears as a function of the dimensions of the image

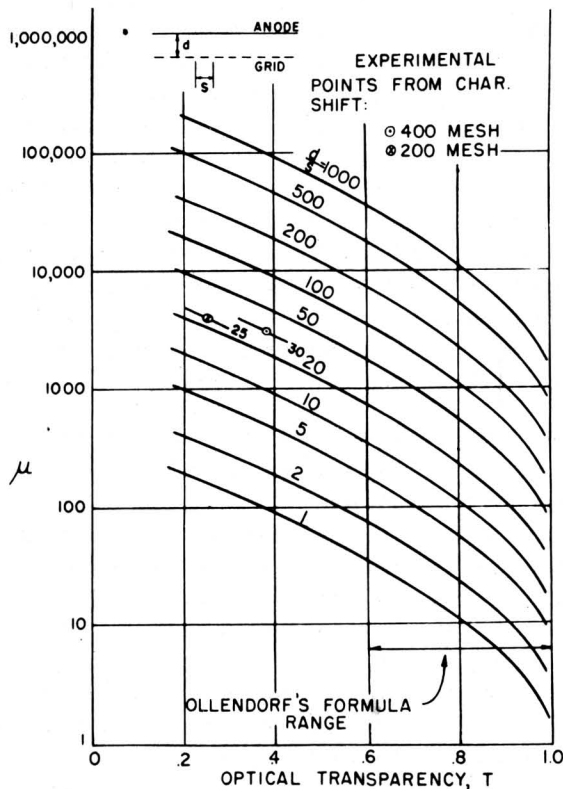


Fig. 17 - Calculated amplification factor as a function of image amplifier dimensions.

corresponding approximately to a $V^{3/2}$ curve. At low current densities (of the order of 0.1 ma/cm² and below), where electron optic current distribution prevails, the slope decreases as the current increases. (see Fig. 4) For the equation of this case, which has been presented so far only in a rather complicated form, see A. Recknagel, *Hochfrequenztechnik und Electroakustik*, 51 (1938) p. 66. Note, therefore, that Eq. (1) does not represent the characteristics of present viewing storage tubes.

amplifier system, which are represented by the amplification factor μ_{43} . For its calculation, Ollendorff's formula¹⁸ is used:

$$\frac{1}{\mu_{43}} = \frac{\ln 2z + z^2}{2a - 2z^2} \quad (2)$$

where $z = \pi \times c/s$; and $a = \pi \times d_{43}/s$.

Using Eq. (2), Fig. 17 shows the amplification factor as a function of the ratio of wire diameter to hole spacing ($2c/s$), for various ratios of anode distance to hole spacing (d_{43}/s). Although Eq. (2) is derived for grids with parallel round wires, it was found from anode current characteristics of experimental tubes to give a sufficient approximation for μ_{43} for both etched and electroformed wire mesh grids*. Due to the fine mesh grid, the amplification factors are somewhat higher (> 500) than the ones in conventional triodes and even in many pentodes, which means that the denominator in the parenthesis in Eq. (1) can be replaced by unity.

The amount of variation in dimensions that can be tolerated can now be estimated. It can be seen from Eq. (1) that these variations produce a maximum percentage of anode current variation near cutoff ($V_3 + V_4/\mu_{43} \approx 0$). If, for example, a deviation of ± 5 percent of the highlight anode current can be tolerated near cutoff, the variations of $2c$ and s should not exceed the order of magnitude of ± 1 percent for large negative values of the space charge grid potential V_3 . From Eq. (1), it can be seen that the background noise due to non-uniform grid dimensions will be more apparent in darker large area gray shades than in brighter ones where it amounts to smaller changes in current density. As can be seen from Fig. 18, this is in agreement with observation. As a result, random variations of the order of only ± 1 percent or ± 5 percent, respectively, are permissible for $2c/s$ and d_{43}/s , for the condition stated above. This implies rather stringent requirements for manufacturing as well as for stretching, mounting, and testing of grids used in image amplifier tubes. Considering the fact that for a 500-mesh grid a few percent variation in grid wire diameter is only of the order of 1 micron, one may also conclude that for the same number of lines per target to be resolved, larger image amplifier systems should have less variable- μ background than smaller ones.

*For example: (a) 500 mesh, electroformed: $d_{43}/s = 10 \text{ mm}/0.05 \text{ mm} = 200$; $2c/s = 0.01 \text{ mm}/0.05 \text{ mm} = 0.2$; μ_{43} calculated: 2200; observed: 2000. (b) 100 mesh, etched: $d_{43}/s = 12$; $2c/s = 0.3$; μ_{43} calculated: 250; observed 232. The agreement is probably due to the larger cross section of the mesh wires, as compared to the circular cross section assumed in (2). Note that (2) is valid (with an accuracy of 2 percent) up to $2c/s = 0.4$ only, and the curves between $2c/s = 0.4$ and 0.6 are extrapolated.

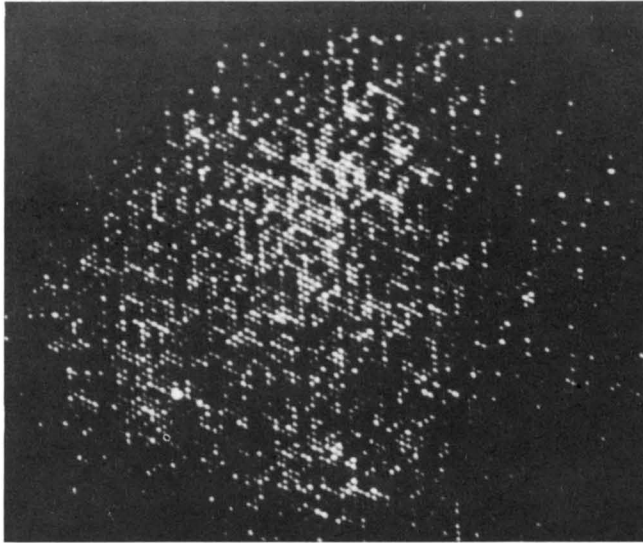
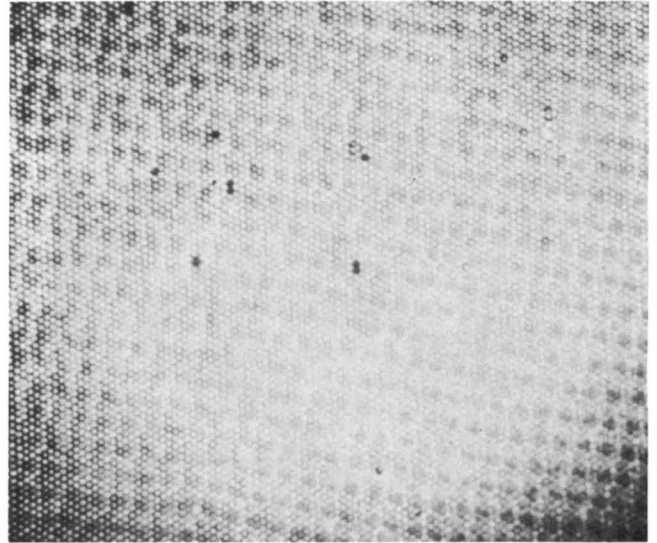
(a) Low viewing beam intensity; $E_{g2} = -37.5$ volts.(b) High viewing beam intensity; $E_{g2} = -16$ volts.

Fig. 18 - Emphasis of background variations in dark areas.

Methods of Manufacturing. Depending on the method of manufacturing, woven, etched, or electroformed mesh grids are in use. In general, they are easily distinguishable by the cross section of their wires.

Photoengraving and Etching. This process has developed from photogravure where variations in gray shade of a photographic image are transferred by a raster to variations in depth or area of corresponding points on a metal plate, which is later used for printing.

For producing fine mesh grids, copper or nickel foils are coated with a "photoengravers resist" paste (e.g., albumen, glue and ammonium dichromate) on both sides. They are then exposed through a raster of opaque dots with accurate registry of the patterns on both sides. Whereas this "resist layer" becomes less water soluble where exposed to light, the dark spots on the metal foil remain soluble and can be washed off with water. After drying and baking of the foil, the unprotected spots on the metal plate are simultaneously etched through from both sides, e.g., by ferric chloride; or by electrolytic etching, e.g., with ferric chloride, sodium acid sulfate, or sulfuric acid.

Although grids up to 1000 mesh per inch have been made by this method¹⁹, they are usually not manufactured with more than 100 to 200 mesh per inch for larger diameters, since the thickness required for mechanical reasons limits their uniformity in contrast to the electroformed grids described below. On the other hand, they are more useful where a low transparency (< 40 percent) or larger hole distances are required.

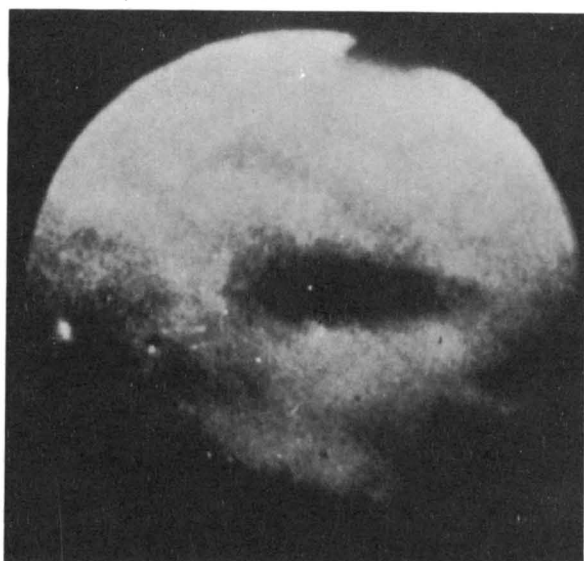
Mechanical Engraving and Electroplating. In this procedure²⁰, a glass is coated with a layer of acid

resist; then lines are ruled through the layer with a ruling engine, and the glass etched for a short time in HF acid to form grooves in the glass where the lines have been ruled. This glass master is now prepared for plating by sputtering metal on it, rubbing it off the surface, and plating the remaining metal in the grooves to form the screen. Cu and Ni screens from 200 to 1500 meshes per inch have been made with a transparency as high as 75 percent (200 mesh), 60 percent (500 mesh), and 50 percent (1500 mesh). Major advantages of this method are: uniformity, high transparency, and very fine mesh.

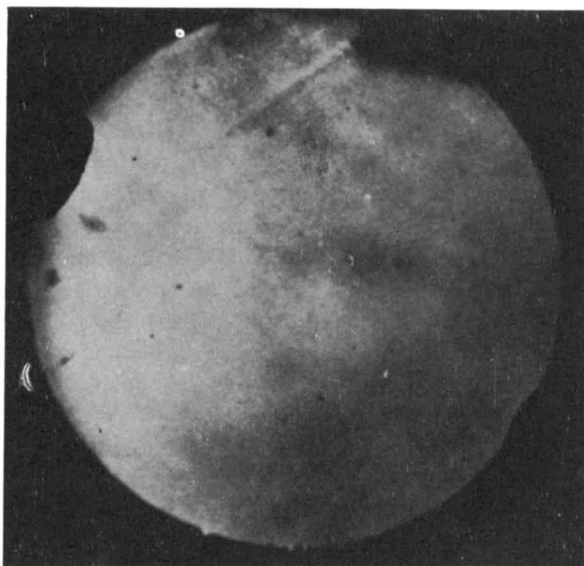
Methods of Tightening. The classical method of tightening fine mesh grids in a heavy frame by stretching it over a sharp edge, and fastening it by clamping or spot welding, is still used. Three other methods have been developed: tightening by heating after welding*, tightening by differential expansion of mesh and frame after soldering*, or tightening by placing the grid between heated metal blocks ("hot blocking")²¹. Each of these methods, if properly applied, allows for tightening of fine mesh screens within admissible variations of μ_{43} . If the tube is to be baked during processing, the expansion coefficient curve of the support ring as a function of temperature should be lower than that of the grid mesh. If this is not

*Approximately 900 degrees C for Cu; see H.B. Law, loc. cit.

*Developed by S.V. Forgue, J.A. Rajchman and P. Rudnick at RCA Laboratories, Princeton, New Jersey. In this process, for example, etched Cu-Ni alloy grids ($a = 16 \times 10^{-6}$) have been used successfully with a stainless steel ($a = 12 \times 10^{-6}$) or Inconel frame. Inconel consists of min. 75 percent Ni + Co, 12-15 percent Cr, and max. 9 percent Fe.



(a) Before demagnetizing.

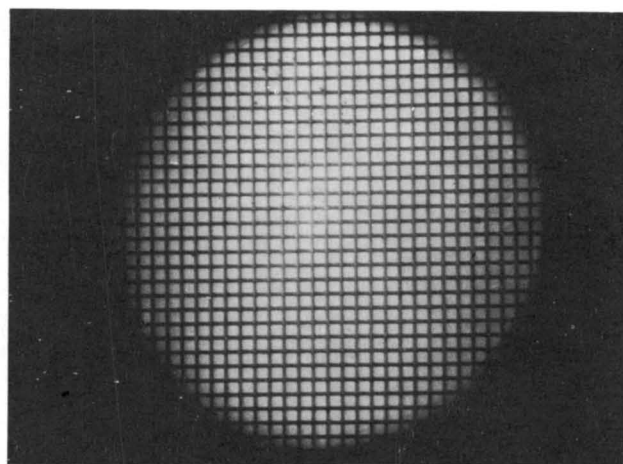


(b) After demagnetizing, showing improved uniformity.

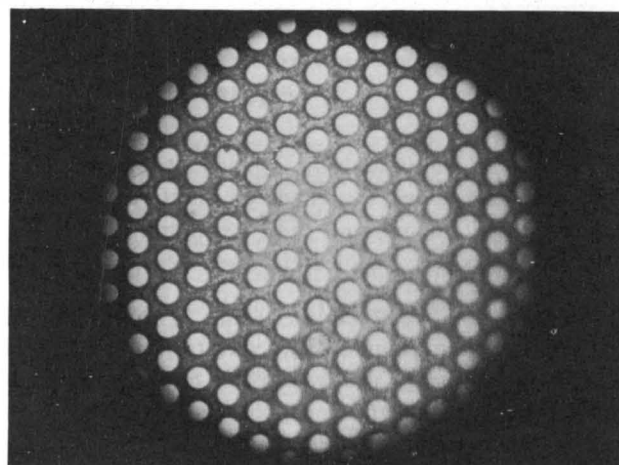
Fig. 19 - Reduction of background patterns by demagnetization (control grid uncoated).

the case, during cooling the thin mesh will cool more rapidly than the frames, thereby overstressing itself, and remain slack at room temperature. Generally, insufficient tightening produces, in tube operation, dark spots for concave, and white spots for convex wrinkles in the mesh, as seen at the luminescent anode.

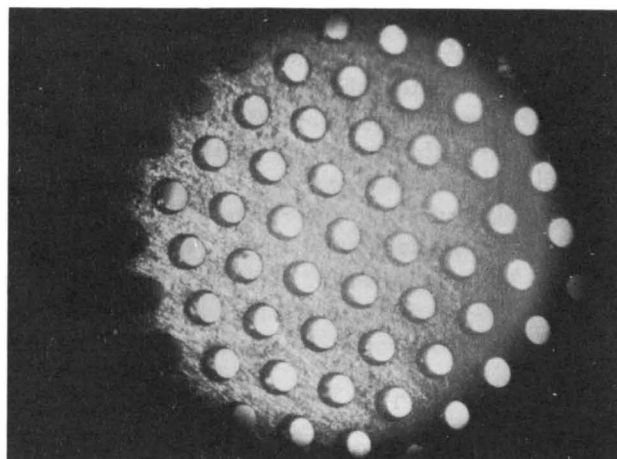
Other dark large area spots (Fig. 19) may be produced by slight magnetic poles in the holding frame which deflect the low velocity viewing electrons near the storage grid. The frame is often made of steel, its expansion coefficient being suitably smaller than that of Cu or Ni mesh. A non-magnetic material like Inconel frequently develops, during the processing cycle of the tube, enough residual



(a) electroformed, 400 mesh



(b) etched, 170 mesh.



(c) etched, with poor registration of resist patterns.

Fig. 20 - Magnified pictures of different fine mesh grids

magnetism to produce such disturbances. Satisfactory results have been obtained using Armco frames, and carefully demagnetizing them rather than using "non-magnetic" Fe-Ni-Cr alloys where the permeability is low, but where a complete demagnetization is difficult.

Testing Methods For Variations in Amplification Factor. It is known that small size mesh grids such as are used in the orthicon can be made nearly uniform enough for television purposes by etching, and adequately uniform by electroforming. Such grids have a thickness of the order of 25 microns. For larger screens (e.g., 4-inch diameter as discussed below), a thickness of 5 microns is desirable for mechanical strength.

By testing variations in amplification factor of such grids, it was found that it was not the difference in dimensions from hole to hole (small area differences) but variations in hole size over larger areas (order of cm^2) which produce the most disturbing variations in μ . As can be seen from Fig. 20, such variations are difficult to recognize in reflected or transmitted light under the microscope and only slightly easier to detect by photographic prints (Fig. 21). Better qualitative results can be obtained by observing the transmitted light coming from a uniform background with the eye. For quantitative measurements, however, a photoelectric measurement of the light transmission,

$$T = (100 - A) \text{ percent}$$

is necessary. (A is the coefficient of absorption in percent, and proportional to the factor $2c/s$ given as a function of the amplification factor μ_{43} in Fig. 17.

A simple but time-consuming method for measuring large area variations in light transmission of fine mesh grids is as follows. The grid is exposed to a light beam, and its surface scanned step by step by an electron multiplier through a narrow (1 mm) aperture mask. as a result, a map of the lines of constant transmission can be drawn. It has been found that for etched grids with 100 holes per inch the large area transmission varies between 30 percent and 40 percent. With variations in A of ± 8 percent, the resulting variable- μ background would be intolerable for half-tone pictures.

A more rapid method for the same purpose uses the same principle but with automatic scanning of the mesh by a light beam intercepted with a Nipkow disc*, and auto-

*Developed by H.O. Hook, RCA Laboratories, Princeton, N.J. The Nipkow disc has 9 holes of 1/8 inch diameter each.

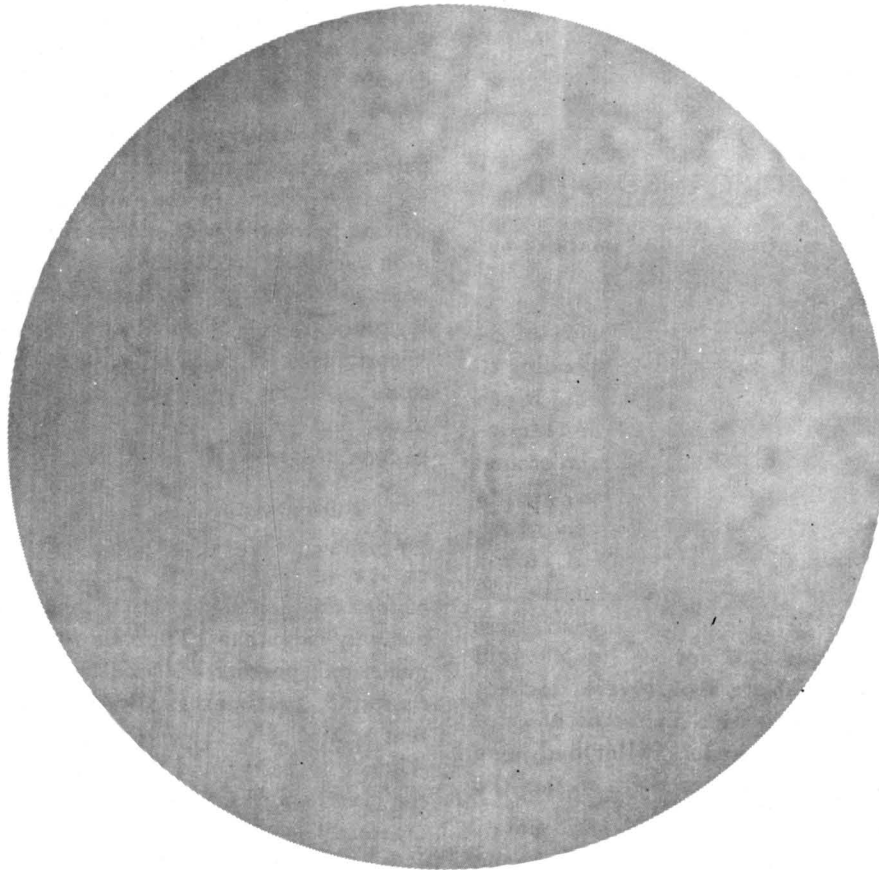


Fig. 21 - Contact print of etched super-nickel grid (100 holes per linear inch, small scale non-uniformities).

matic recording. In Fig. 22, an example is given for a comparison of a 170-mesh etched grid, and a 400-mesh electroformed grid. The recordings on top are taken without a grid, and are used for calibration of transmission. The rounded corners of the pulse are due to the finite diameter of the aperture, and must be deducted from the range of variations recorded for the grids.

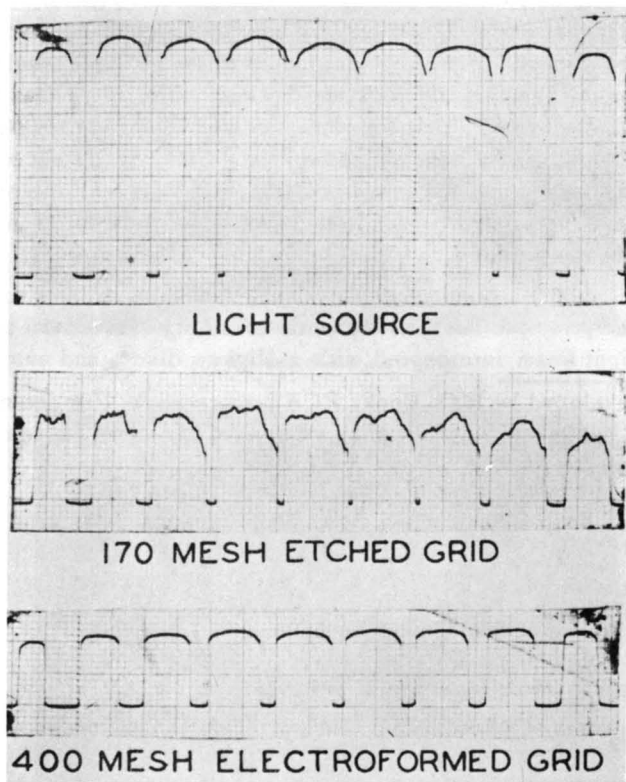


Fig. 22 - Light transmission of metal grids measured by Nipkow scanning method.

The etched grid shows a mean transmission of 34 percent, and variations of ± 29 percent, corresponding to variations in mean absorption, A_m , of ± 15 percent. It can be easily recognized from the recordings that the electroformed mesh shown is much more uniform than the etched one. Its average transparency, T_m , is 37 percent, and its variations are ± 2.5 percent of T_m , or ± 1.5 percent of A_m , which is ten times less than the variations in A_m found for the etched grid. This result is typical for the 100 grids* with 100 to 400 holes per linear inch investigated. One may, therefore, conclude that for 100 to 500 grid wires per inch, and target diameters of several inches, large area variations of amplification factor of electroformed grids are one order of magnitude smaller than those of etched grids*. This is partly due to the fact that the

*Manufactured by Buckbee Mears Co., St. Paul, Minnesota.

*If the large area non uniformities due to etching are caused by physical or chemical non-uniformities of the metal (in our case a Cu-Ni alloy) or by the etching agent, or the resist, this ratio may be improved considerably in favor of the etched grids.

holes of grids etched from two sides are not cylindrical or prismatic for rectangular holes but exhibit the shape of two cut cones or two cut pyramids with a thin edge. This becomes more evident at poor registration of the two patterns (Fig. 20c). As a result, small variations in dissolved material or in thickness produce larger variations in transmission as compared to electroformed grids.

One may also conclude that, because it is possible to manufacture electroformed grids with variations in amplification factor of the order of ± 1 percent, image amplifier tubes with screen diameters of 1 to 5 inches may be built with a sufficiently low variable- μ background pattern, so far as the metal grid support of the storage grid is concerned. In any case, accurate and rapid testing methods are necessary to determine the variations in μ of each individual grid before it is finally mounted in the image amplifier system.

Storage Layers

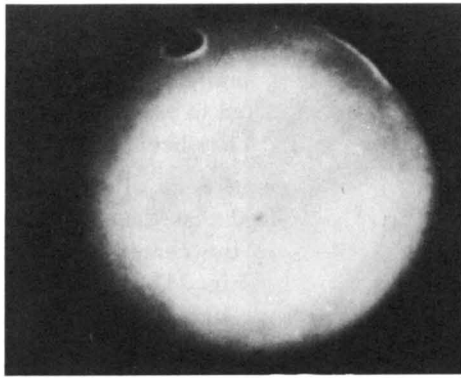
General Requirements For Uniformity, Especially of Secondary Emission. The storage layers applied to the supporting metal control grid of an image amplifier system may produce undesired background patterns due to nonuniformities in thickness, dielectric constant, secondary emission, or bombardment induced conductivity. As an example, only requirements of secondary emission will be discussed.

It should be noted first that undesired background patterns due to nonuniform secondary emission may be greatly reduced in the writing process, if equilibrium writing below the second crossover of the secondary emission curve, or bistable writing with the aid of a holding beam are used²². The same is true for equilibrium erasing processes. The problem of nonuniformity is especially important for all nonequilibrium writing and erasing operations of image amplifier systems, which are frequently used, and for equilibrium writing and erasing above the second crossover.

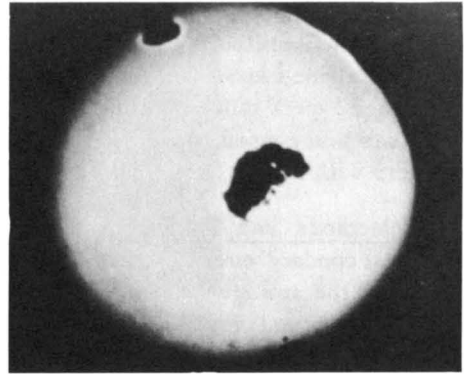
Furthermore, in order to limit secondary emission background patterns to less than 10 percent variation of charge in the written picture, the current, $i_{coll} - i_{pr}$, which charges the storage layer during writing, should not vary more than 10 percent during writing. As the same numerical percentage variation in secondary emission factor, δ , produces smaller variation of the charging current at high δ 's, the use of insulators with δ 's large with respect to unity, and operation of the writing beam near the maximum of the secondary emission curve are advantageous*.

Preparation. The insulating storage layer may be applied to the metal grid surface by evaporation in a high

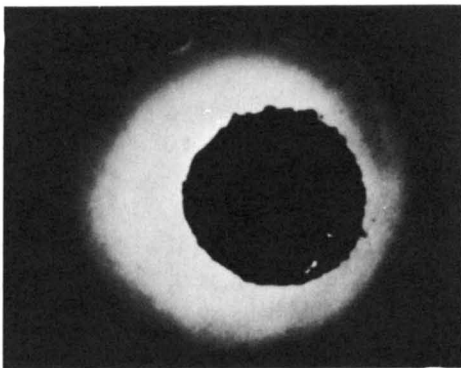
*These conditions are also favorable for obtaining a high writing speed.



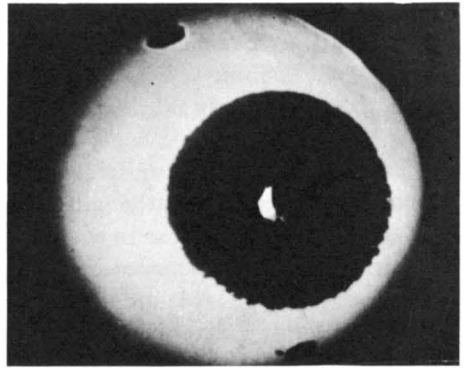
$V_{g2} = 50$ VOLTS
(a)



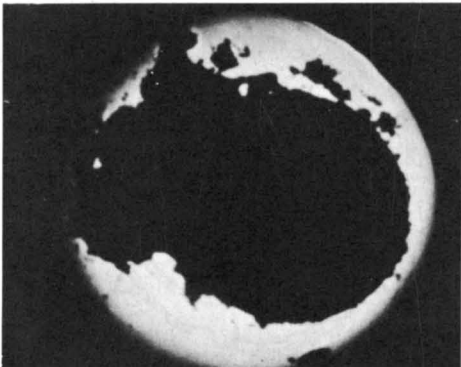
$V_{g2} = 40$ VOLTS
(b)



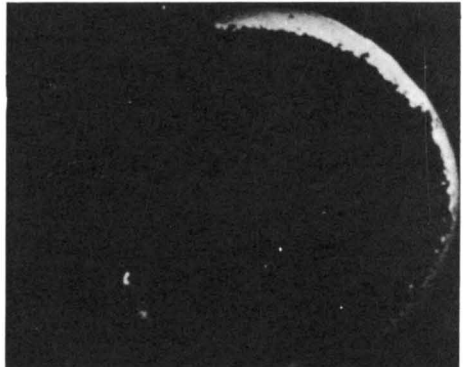
$V_{g2} = 35$ VOLTS
(c)



$V_{g2} = 30$ VOLTS
(d)



$V_{g2} = 25$ VOLTS
(e)



$V_{g2} = 20$ VOLTS
(f)

DARK AREA BELOW, WHITE AREA ABOVE FIRST CROSSOVER

Fig. 23 - Bistable secondary emission patterns (lines of constant first crossover potential) for magnesium fluoride layer.

vacuum (usually in a bell jar), by the ethyl-silicate process²³, by floating methods²⁴, or by spraying. Materials are silica²⁵, magnesium-fluoride²⁵, calcium fluoride²⁶, alumina and crystalline zinc-ortho-silicate²⁷. The thickness of the storage layers range from 0.25 to 100 microns, the larger values being used mostly for black-and-white image amplifiers with holding action.

Testing Methods and Their Results. Major non-uniformities in secondary emission factor, δ , may be detected by scanning the storage layer with the writing beam, and observing the signal received from the supporting metal grid ("backplate"), or a collector, with a television receiver²⁸. This method is very useful for survey purposes, but its accuracy is generally limited to a few percent change in the secondary emission factor of the insulator²⁹.

Although this accuracy can be considerably improved by the use of an auxiliary beam charging the storage layer under a non-equilibrium condition³⁰ a more sensitive testing method is possible. In this method, instead of a secondary emission current pattern, a background equipotential map is used as a measure for uniformity. This is accomplished simply by bombarding the storage layer with one of the beams at a velocity close to the first or second crossover potential of the secondary emission curve of the insulating material. Storage layer areas with a secondary emission factor smaller or greater than unity will then appear as black or white areas, respectively, on the luminescent screen. Because of the bistable nature of this process, and the image amplification, high sensitivity is obtained.

First Crossover Background Equipotential Mapping Using Bistable Writing. For these patterns, one collimated (viewing) beam of the spray type was employed in a direct-view storage tube such as shown in Fig. 2. For writing, the storage layer surface is first completely discharged (erased) by connecting the storage mesh, G_2 , first with the collector grid, G_1 , and then switching it to the spray beam cathode potential. Assume that the center of the storage grid has a higher first crossover potential than the edge. If the backplate is then shifted to a positive potential (with respect to viewing cathode) near the first crossover potential, the center, which is below first crossover, is shifted to viewing cathode potential, whereas the edge, where electrons land above the first crossover, is shifted to the positive collector potential. As a result, the location of the elements of the layer which are exactly at crossover potential is indicated by the borderline between a bright center area* and a slightly darker region on the edge of the screen. This picture, therefore, (appear-

*Because more of the slow electrons in front of the negative center area are drawn through the storage grid holes, as compared to the electrons in the outer positive area.

ing as a weak negative of Fig. 23) gives the contour of the bistable δ -pattern for a backplate of 30 volts and represents a line of constant secondary emission. A much higher contrast ratio of this pattern is obtained by "viewing", where the backplate is again switched to viewing cathode potential after the bistable pattern has been established.

After this switching, the edge of the storage grid, being more positively charged than the center, transmits viewing electrons, whereas the center, being negative, does not (positive picture of Fig. 23). Other lines of constant crossover potential are obtained by repeating this process with lower or higher backplate voltages (20 to 50 volts in the examples given in Fig. 23). These patterns are stable and reproducible. In Fig. 24, they are assembled to an equipotential map of this particular MgF_2 coated storage grid. If the secondary emission is uniform and the errors of collimation axially symmetric, these equipotential contours should form a set of concentric circles, the potential difference between the edge and the center area being only a small fraction of the control potential range on the storage layer (e.g., several volts for a range of 30 volts). Each non-circular shape of the equipotential contours, and each larger range of equipotentials indicates non-uniformities of secondary emission in corresponding areas. From Fig. 23, e.g., (if no axially asymmetrical aberrations of the collimating lens are present) one may conclude that the center and the edge of the storage grid exhibit more non-uniformities than the area between them. Also, it can be seen that the maximum equipotential difference from which the non-uniformity may be estimated, is in this map about 20 volts, and is thus much too large.

A much more uniform secondary emission was obtained if the target during processing was electron bom-

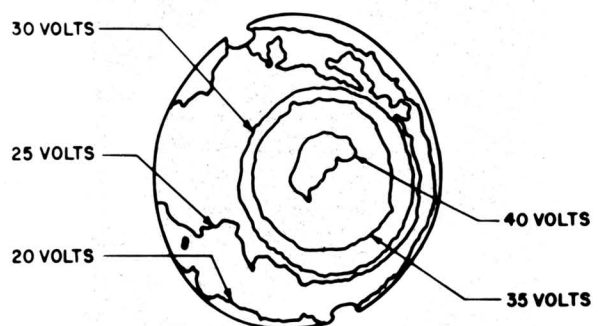
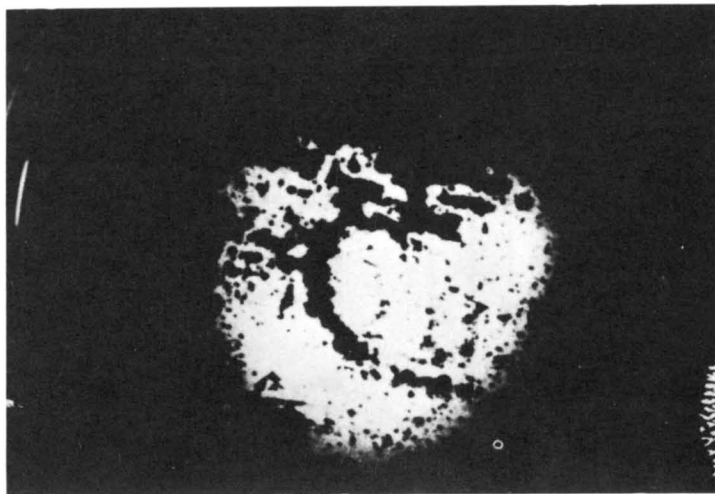


Fig. 24 - First crossover potential map.

barded only at room temperature and not while hot. In this case, the maximum equipotential differences of the δ -patterns were found reduced to several volts. Besides, an interesting effect of an increase of secondary emission* of MgF_2 during several hours bombardment has been

*So far, only a decrease of δ under electron bombardment has been reported. One explanation for this increase would be the disappearance of monatomic gas or vapor layers absorbed at the surface.



BEFORE BOMBARDMENT

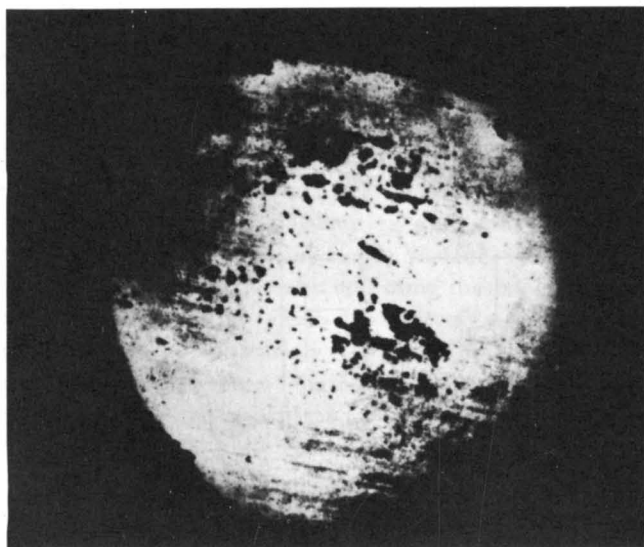
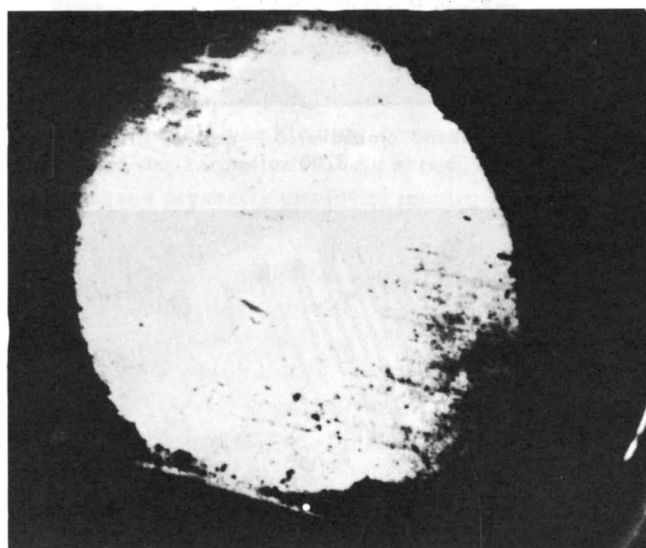
AFTER FIRST
BOMBARDMENTAFTER SECOND
BOMBARDMENT

Fig. 25 - Shift in first crossover with bombardment (storage layer sprayed with 31 volt electrons in all cases).

observed (Fig. 25). Before bombardment, there are relatively large dark areas, indicating regions below first crossover. After the first bombardment, there is more bright area, showing that some of these areas have gone above first crossover. After the second bombardment, there is still more bright area.

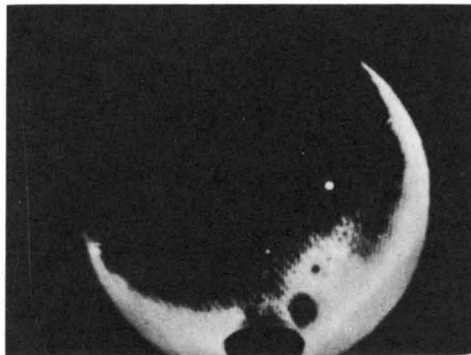
Second Crossover Background Equipotential Mapping Using Equilibrium Writing. For second crossover equipotential maps, viewing and writing beams have been used simultaneously. The storage layer is first completely discharged, as described for the first crossover equipoten-

tial maps, and the viewing beam adjusted with the backplate near viewing cathode potential, as is necessary for regular viewing.

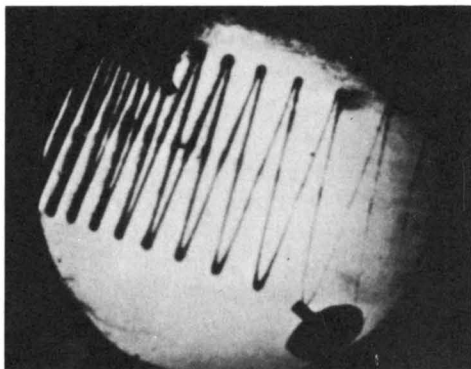
After this, the writing beam is adjusted so that electrons land at the storage surface with an energy which is slightly below second crossover (2.8 kv for silica, for example). Then, by increasing the writing beam cathode voltage step by step, equipotential δ -patterns are obtained. However, because no bistable holding action is involved, the equipotential line is more diffuse, and the contrast ratio smaller than in the first crossover δ -patterns (see



(a) second crossover potential map



(b) second crossover δ - pattern written at 3700 volts



(c) stored oscillogram

Fig. 26 - Patterns showing correlation of non-uniformities in crossover potential and in writing:

Fig. 26). The equipotential map of second crossovers as shown in Fig. 26a bears but little resemblance to the first crossover map of the same target (Fig. 24), indicating that non-uniformities of secondary emission in surface or volume can be distinguished³¹.

Any general conclusions as to the specific influence of storage layers with irregular δ -patterns upon the stored images must be checked on a larger number of storage tubes. However, the superposition of a δ -background pattern obtained by this method upon an oscillogram written above second crossover on this silica target can clearly be seen in Fig. 26b and c. Here, the area where the second crossover potential is highest is also the area where

the written pattern is weakest in the stored image. The crescent-shaped contour of the δ -boundary of Fig. 26b results mainly from the fact that the writing beam is inclined at an angle of 15 degrees to the tube axis*.

The degree to which it has been possible to reduce variable- μ and secondary emission background patterns in stored half-tone pictures may be judged from Fig. 36.

Storage Surface Potential Shifts During Operation

The processes of writing and erasing depend on potential shifts of the target surface involving the action of secondary emission. Before discussing these processes the secondary emission charging processes of an electron-bombarded insulator will be summarized. In Fig. 27 is shown an electrode system with an insulating target bombarded by an electron beam. The secondary emission curve of an insulator is shown in Fig. 28 as a function of the bombarding energy of the electron beam. For an insulating target as in Fig. 27, the surface potential may be initially arbitrary so that the bombarding energy of the primary beam is determined by the difference in potential

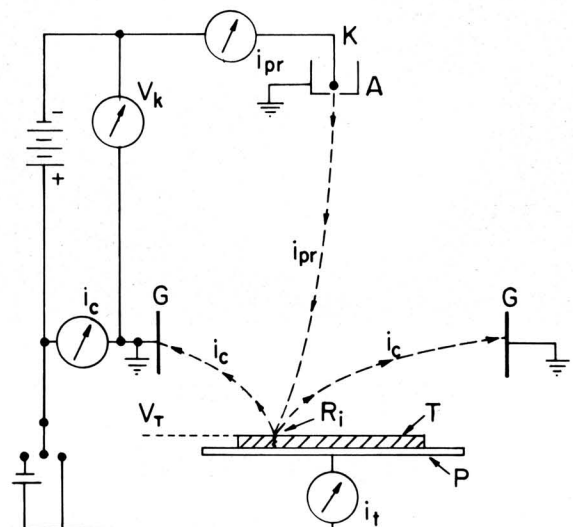


Fig. 27 - Typical electrode arrangement for an electron-bombarded storage target.

*The large difference in second crossover equipotentials (4.2-2.8 = 1.4 kv) over the storage layer area, therefore, mainly indicate differences in secondary emission due to different angles of incidence of the writing beam (5 to 25 degrees from the tube axis). For comparison, see, e.g., secondary emission and crossover potentials for A1 as a function of beam angle of incidence in H. O. Mueller, Z. F. Physik, 104 (1937) p. 480; in his curves for A1, changes of angle of incidence between 2 and 25 degrees produce a 20 percent change in secondary emission.

between the target surface, V_T , and electron gun cathode potential, V_k . Also, the secondary electrons emitted from a bombarded target point, most of which have only a few volts of energy, can leave the neighborhood of the target surface only if there is no large decelerating field between the target and collector. The charging of the surface of an insulating target element is thus dependent upon the secondary emission ratio, δ , and whether or not the emitted secondaries are allowed to escape from the target element.

Assuming an electrode arrangement as shown in Fig. 27, bombarded insulating target elements will have equilibrium potentials determined by the cathode potential of the electron gun, and the initial surface potential. The loci of these equilibrium potentials is indicated by the heavy lines of Fig. 29. In addition to the equilibrium potentials, Fig. 29 shows the direction of charging of an insulating surface with arbitrary initial potential, V_T , bombarded with electrons from a cathode at a potential, V_k . It is thus called the *potential shifting diagram*. The shape of the equilibrium curves as well as the reasons for the directions of potential shift are discussed elsewhere³². For desired potential shifting any point on the diagram can be chosen by (1) selecting a specific cathode potential of the bombarding gun, and (2) setting the potential of the insulating target surface. The second step may be accomplished by selecting the backplate (or storage mesh) potential which capacitively sets the storage surface at approximately the same potential. This can be done by inserting a battery, for example, between the collector and the backplate as shown in Fig. 27, or by pulsing, or both.

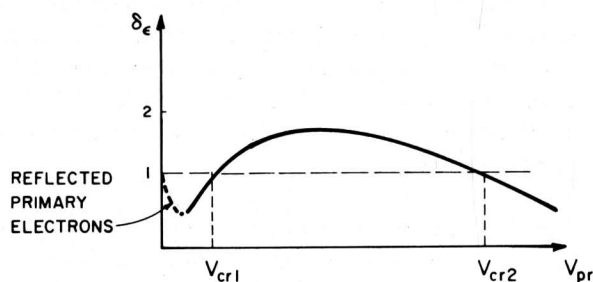


Fig. 28 - Typical secondary emission curve: secondary emission ratio, δ , as a function of bombarding primary electron energy, V_{pr} , at the target.

In the direct-view storage tube (Fig. 2) the storage target is perforated, unlike the target shown in Fig. 27. The secondary electrons emitted by such a perforated storage layer may be collected by three different positive electrodes: the collector grid on the gun side of the storage grid, the supporting mesh, and the luminescent anode. This arrangement makes equilibrium writing (backplate or collector modulation) difficult since the storage mesh

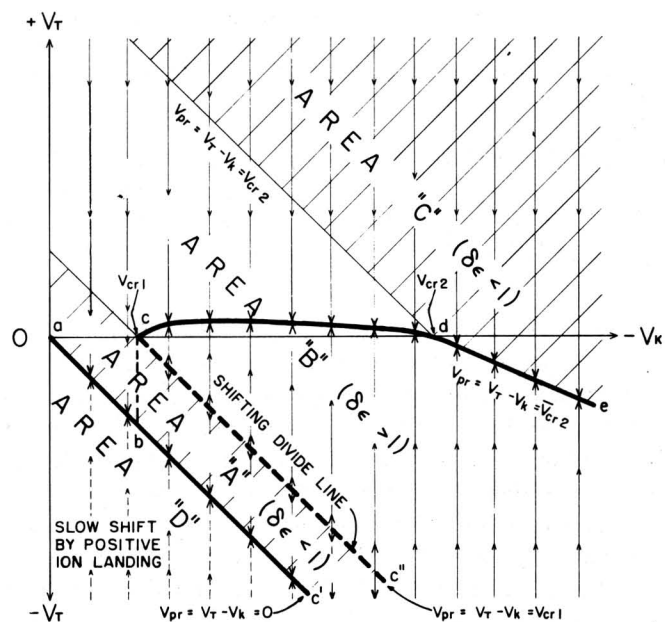


Fig. 29 - General potential shifting diagram.

tends to act not only as a backplate but simultaneously as a collector due to the close spacing between the insulating surface and the target mesh. As a result, all of the writing processes presently employed require modulation of the writing beam current (non-equilibrium writing).

Three types of operation are possible with present viewing storage tubes: bistable operation (on-off), bipotential operation (on-off), and halftone operation. The first two methods are preferable for telemetering, teleprinting, certain types of radar, oscilloscopes, and computers; the third is necessary for television, high quality radar, and high quality oscilloscope applications. In all three types of operation, erasure can be accomplished either by erasing all storage elements simultaneously (over all erasure) or by erasing a few elements separately (spot erasure)³³.

Bistable Operation

In this type of operation, a black-and-white or on-off picture is produced by shifting the storage surface to either one of two potentials: (a) a potential close to collector potential, corresponding to white levels (level 0 or 1' in Fig. 30), or (b) viewing gun cathode potential, corresponding to black levels (e.g., level 4 in Fig. 30). This requires the setting of the cutoff of the control characteristic to viewing-gun cathode potential. The characteristic is then in the range of storage surface potentials that are *positive* with respect to the viewing-gun cathode potential (Fig. 30). The required vertical position of the characteristic ($V_T = -30$ to 0 volts in Fig. 30 as compared to $V_T = -40$ to -30 volts in Fig. 32) can be provided by:

- (1) A relatively high amplification factor (e.g., a fine storage mesh),

Viewing Storage Tubes

- (2) A low gradient between storage grid and phosphor,
- (3) A high gradient between storage grid and collector,
- (4) A small gradient across the storage insulator (e.g., by operating the storage mesh at lower positive potentials than it is operated in bipotential or half-tone operation described below).

The writing process in bistable operation is derived from a bistable (holding) storage mechanism described by Haeff³⁴ for a viewing storage tube without a control grid³⁵. For the equilibrium curve a-b-c-d', a first crossover potential of 20 volts is assumed. The 45-degree "shifting divide", therefore, intersects the V_k axis at this abscissa value. Furthermore, a writing beam cathode potential, V_k , of -3000 volts with respect to the collector is assumed, and a potential of -30 volts for the cathode of the flood beam, which is identical here with the holding and viewing beam. For convenience, the equilibrium curve is shortened between c and d'; states (levels) of the floating potential, V_T , significant for shifting are indicated by horizontal lines and the shifting steps are indicated by Roman numerals with a sequence according to operation.

As an example, suppose that the storage layer potential is close to the equilibrium potential line b-c'. In this state, the positive ions landing at the storage surface tend to drive its potential positive (lower arrow) against the much larger action of the flood beam which tends to drive the overall potential of the storage surface towards the line b-c' (upper arrow). Therefore, the whole target surface has a uniform negative potential of -30 volts with respect to the collector; few holding beam electrons land on it, and practically no electrons arrive, at the luminescent screen.

In writing, the action is along the line $V_k = -3000$ volts. When the writing beam is switched on (if the electron density in its spot is larger than the holding beam density and the writing beam is on long enough) there occurs a transition (I) from level (4) to level (1), establishing a more positive potential at the storage grid surface by secondary emission. Level (1) may be as high or even higher than the horizontal branch c-d' of the equilibrium potential curve, where the storage surface potential is about equal to the collector potential. It is only necessary, however, to shift level (1) above the value of V_T on the "shifting divide" at $V_k = -30$ volts (level (2)) since the hold-view beam will do the rest of the shifting (from level (1) to level (1')) automatically by secondary emission (transition (II)). The two arrows indicate the holding action which occurs at this level for storage grid areas corresponding to white picture areas.

A white equilibrium potential has now been established for all storage grid areas which have been shifted across the divide by the scanning writing beam, whereas all other areas remain stable at level (4), producing dark tones. This bistable condition can be maintained for any length of time, since the charges on the storage surface corresponding to black-and-white phosphor areas are constantly renewed by the view-hold beam.

On the right side of Fig. 30, the viewing current characteristic is shown. Level (4) corresponds approximately with the cutoff voltage. Due to a low flood beam voltage, and a low voltage gradient across the storage layer, a large part of the characteristic extends into positive values of storage grid surface potential, V_{2s} . As a result, at white equilibrium levels, (1'), the storage grid surface is at collector potential, and is continuously bombarded by flood beam electrons of considerable energy.

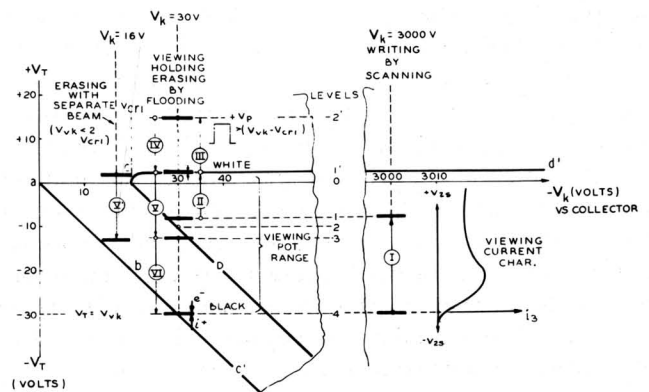


Fig. 30 - Potential shifts for bistable operation.

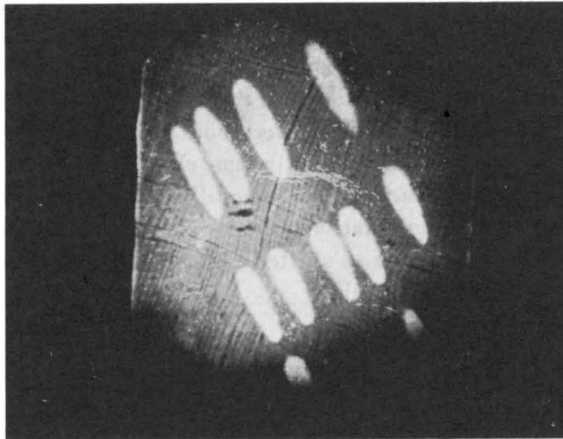
To avoid high gradients at the edge between white and black storage elements, potential differences of less than 100 volts are desirable, limiting the value of V_k . Also to prevent breakdown through the target, V_k should be maintained below a level of 50 volts per micron thickness of the target.

Erasing may be accomplished by pulsing in a positive direction either the cathode of the flood beam or the backplate; thus establishing a negative potential on the storage grid surface by electrons landing during the pulse. Fig. 30 indicates transition from level (1) to level (3). This potential shift must be sufficient to shift the surface below potential level (2); from there, the flood beam, by secondary emission shift (VI), pushes it down to the lower equilibrium state (level (4)), which completes the write-hold-view-erase cycle. Maximum erasing speed is obtained if the capacitive shift moves the dark equilibrium level (1').

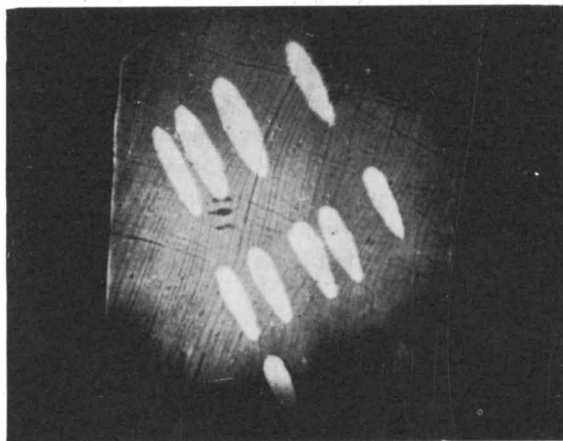
Transition (V) may also be accomplished without pulsing by a special erasing gun with a cathode voltage,

which shifts V_T from level (1') to level (3) (Shift V'). For spot erasing, V_k must be less than $2V_{cr1}$ otherwise the erasing beam with its cathode potential below V_{cr1} cannot push white areas over the potential divide.

In Fig. 31 a picture is shown which was obtained with a direct-view storage tube after 10 sec. and after 5 hours. The picture was produced by deflection of an astigmatic defocused writing beam. It was found that even after 24 hours, the original picture pattern remained unchanged if constant density of the holding beam was maintained.



(a) viewing duration, 10 seconds



(b) viewing duration, 5 hours

Fig. 31 - Picture obtained with bistable operation.

The main advantage of bistable operation as described is the possibility of extended viewing, which is desirable, for example, in oscillography. Disadvantages, other than the limitation to black-and-white operation, are the relatively high bombarding velocity of the holding beam electrons in white picture areas which reduces the life of the storage layer (after-images), and the relatively large potential difference between white and black storage surface areas which deteriorates resolution and limits the viewing duration. Storage layers of the order of 10 microns

are desirable to withstand the potentials required. Furthermore, the maximum writing speed with bistable operation is considerably less (approximately 10^5 spots per sec) than that for non-holding bipotential operation (approximately 10^8 spots per sec) since the potential shift necessary for writing is usually much larger. The erasing process is slower, not only because of the larger potential shift, but also (in the case of spot erasing) because the erasing gun cathode voltage is limited to values less than V_{cr1} .

Bipotential Operation

In this type of operation a black-and-white or on-off picture is produced by shifting the storage surface to either one of two potentials: viewing gun cathode potential, V_k , (corresponding to white levels), or a more negative potential beyond the cutoff of the storage grid (corresponding to black levels). Whereas, in bistable operation as discussed above, the black level corresponding to the cutoff of the viewing beam characteristic is set at the potential of the viewing beam cathode, the black level in bipotential operation is set below this level (level (4) of Fig. 32). Also the range of write-view storage layer potentials in bipotential operation (levels (2) to (4)) is smaller than the range of potentials in bistable operation (between $V_T = -30$ and $V_T = 0$ volts in Fig. 30).

While in bistable operation erasing with a separate beam can be accomplished only with a low-voltage erasing gun ($<V_{cr1}$), as previously mentioned, this restriction does not exist for bipotential operation as shown in Fig. 32 since all levels remain below the "shifting divide" during operation.

The positioning of the control characteristic in bipotential operation so that it is in the range of potentials negative with respect to the viewing-gun cathode, V_k , can be achieved by:

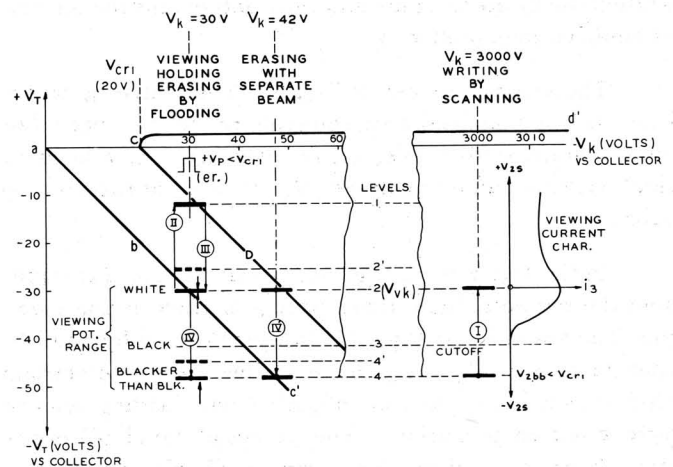


Fig. 32 - Potential shifts for bipotential operation.

Viewing Storage Tubes

- (1) a relatively low amplification factor (e.g., a coarser storage mesh),
- (2) a high gradient between storage grid and phosphor,
- (3) a low gradient between storage grid and collector,
- (4) a considerable gradient across the storage insulator (e.g., by operating the storage mesh at higher positive potentials).

As in Fig. 30, a writing beam cathode potential of -3000 volts is assumed, and a potential of -30 volts for the cathode of the flood beam in its viewing and holding function. Assume that initially the entire storage layer is at a uniform negative potential, indicated by level (4). Because of the limitation of the erasing pulse voltage ($V_p < V_{cr1}$), the storage grid surface potential (with respect to viewing gun cathode), V_{2s} , at level (4) (V_{2bb}) cannot be larger than V_{cr1} ($V_{2bb} < V_{cr1}$). Thus, depending on V_{cr1} and the length of the viewing current characteristic, level (4) may be considerably more negative than level (3) which corresponds to the cutoff potential of the characteristic. Level (4) is therefore called "blackier than black".

The practical value of using level (4) instead of level (3) as a black potential level consists in obtaining a longer viewing duration. During viewing, positive ions produced by the viewing beam land at the storage surface causing a continuous positive shift at levels below the equilibrium line $a b c'$. If level (4) is used as a black level, considerable time will elapse before the ions shift the potential from this level to the cutoff potential (level (3)). In contrast to this, if level (3) is used as a black level any positive shift from this level will appear immediately as a gray background, with a reduction of contrast in the picture. In practice, an increase of viewing duration by a factor of approximately two has been observed when using level (4) instead of level (3). The increase depends on the ratio of white to black areas since this ratio determines the amount of positive ions produced.

The writing process in Fig. 32 is indicated by transition, I. The potential corresponding to "white" phosphor area is shifted from level (4) to level (2), which is identical with the cathode voltage ($V_k = 30$ V) of the viewing beam.

In the left part of Fig. 32, levels (2) and (4) represent the two potentials at the storage surface during viewing. The potential of level (2) (white) is fixed by equilibrium holding to $V_T = V_k$ since landing viewing electrons shift it constantly to more negative and landing ions to more positive potentials. The potential level (4) is not fixed because positive ions drive it slowly toward collector potential, during viewing. This shift is not noticed

insofar as it occurs beyond the cutoff level (3). However, for viewing durations greater than 1 minute, continuous, holding of level (4) may be accomplished by continuous pulse erasing (see below).

Erasing is accomplished by increasing the velocity of the electrons landing at the storage surface by an amount equal to the potential difference between level (2) and (4) for a length of time which is sufficient to charge the storage surface to its original potential (level (4)). This may be accomplished by repetitive positive pulses applied to the storage grid. If rectangular pulses are used their amplitude must be less than V_{cr1} to avoid crossing of the potential shifting divide by the white level. The leading edge of the positive pulse (transition (II)) drives the white as well as the black level into the area between line $a b c'$ and the shifting divide where both levels are charged negatively by landing flood beam electrons (transition (III)), until they reach the same equilibrium potential (level (2)). At the termination of the pulse (transition (IV)) the former white area is shifted back to level (4) and becomes a black area again.

The effect which was achieved here by pulsing the backplate positive, can also be accomplished by pulsing the flood beam cathode negative, or by employing a separate erase beam with a more negative cathode voltage. Shifting by the latter method is shown in Fig. 32 as transition (IV'). Compared to bistable erasing, the erasing beam cathode voltage can be greater than V_{cr1} , which makes the design of electron guns for spot erasure much easier.

Half-tone Operation

The shifting cycle of the half-tone operation to be described here is analogous to the bipotential on-off operation discussed above, but does not include the "blackier-than-black" level.

In Fig. 33, for greater clarity, the operation is separated into four different diagrams: (a) erasing, IV; (b) writing and viewing, I; (c) erasing, II; (d) erasing, III. The level numbers (Arabic) and shift numbers (Roman) correspond to the ones for Fig. 32.

The requirements for the position of the viewing current characteristic are the same as outlined for the bipotential on-off operation. For half-tone operation linearity of this characteristic is desirable. In Fig. 33, six distinguishable half-tones are assumed.

Fig. 33 shows the black level (3) which remains after the last step of erasing (by flooding or separate beam) over the whole storage grid surface. The viewing beam cathode potential, V_k , is adjusted so that this level is identical with the cut-off potential of the viewing beam characteristic. By non-equilibrium writing (primary cur-

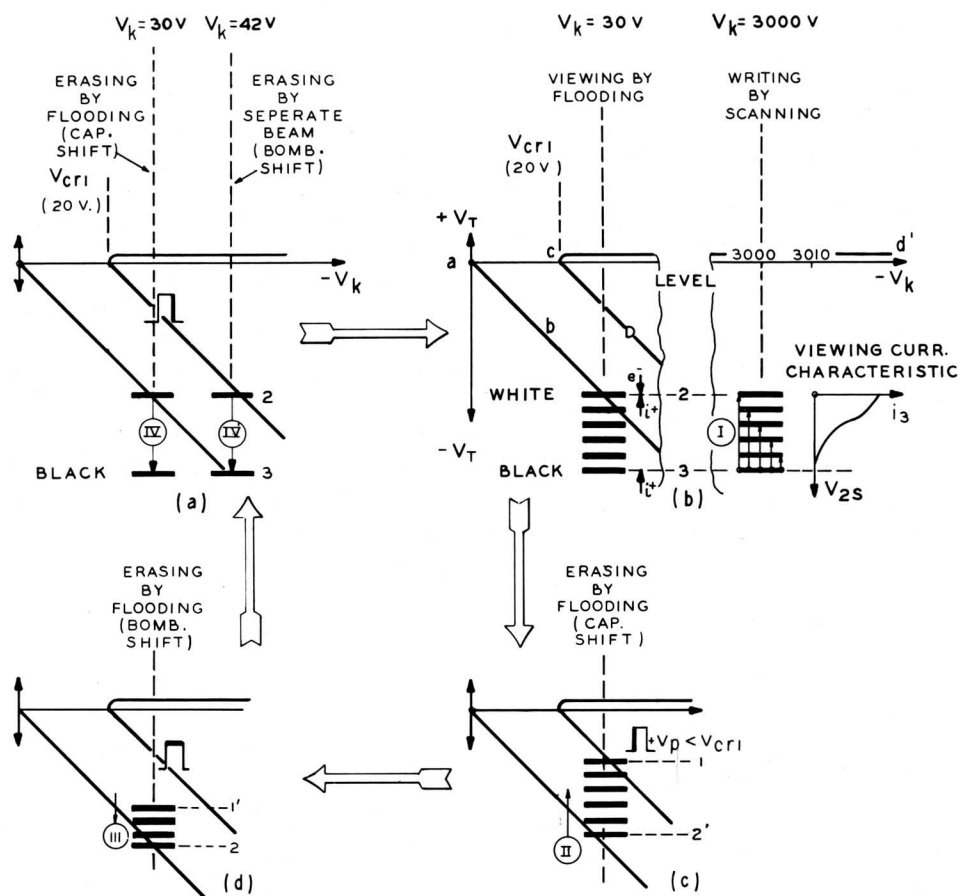


Fig. 33 - Potential shifts for halftone operation.

rent modulation) (Fig. 33, $V_k = -3000$), five half-tone levels are established above level (3), the highest corresponding to the end of the useful characteristic.

In the left part of Fig. 33, levels between level (3) and (2) represent a half-tone scale of storage surface potentials during viewing. As in the bipotential operation, level (2) (white) is stable, whereas level (3) (black) moves slowly to more positive values due to ions.

Because of the absence of a blacker-than-black level (such as level (4) in Fig. 32), this "creeping" of level (3) is noticed as a change of black to a grey and, frequently, as a less uniform background than in bipotential operation. Therefore, compensation or holding methods are more important for half-tone operation than for bistable operation.

Analogous to the erasing process described under bipotential operation, the first step of flood or overall erasing (transition (II) in Fig. 33c) consists in a capacitive shift of all levels (by the leading edge of a positive pulse) into the area between the divide and the line $a b c'$. Thus, the former black level is shifted to level (2'), above the former white level (2). Since the pulse height is limited to $V_p < V_{cr1}$, this former white level is below the divide (at level (1)) after this shifting.

The second step of flood erasing (transition (III) in Fig. 33d), which occurs during the pulse, consists of a common downward shift of all half-tone levels under flood beam bombardment. Because level (2) is "locked", they shift one by one to this level ($V_T = V_k$), until finally only level (2) remains. The third step of flood erasing (IV in Fig. 33a) is again a capacitive shift of this remaining level (2) to the cut-off level (3). This occurs at the end of the pulse.

The erasing steps of Fig. 33 may be avoided by using a separate erase beam with a cathode voltage, $V_{ek} = V_{vk} + V_{cut-off}$, where V_k is the flood (viewing) beam voltage. The action of this beam drives level (2) directly negative to level (3) (transition (IV') Fig. 33a). Such a separate erase beam is advantageous for spot or line-by-line erasure.

Viewing Duration and Methods for Increasing It

Effect of Ions on Viewing Duration.

For this section, define viewing duration T_v as the time required for the background of a single pattern to in-

Viewing Storage Tubes

crease to 10 percent of the maximum highlight brightness. In a half-tone picture, this corresponds practically to an increase (ΔV_{2s}) of the storage layer potential, V_{2s} , (with respect to the viewing beam cathode potential) of dark areas by 10 percent of the useful characteristic range.

For most applications, including radar, viewing durations of 10 to 20 seconds are more than adequate. Viewing durations of 0.1 second are adequate for television applications. Most insulators suitable for storage grids, like silica or magnesium fluoride, will maintain a charge of a few volts for weeks if the tube is not operated. The factor which limits the viewing duration in the normal operation of a tube is not insulator leakage, but the landing on the grid of positive ions produced by the viewing-beam, which discharge the storage grid capacitance. The viewing duration is given by the equation

$$T_v = \frac{\Delta V_{2s} C_t}{i^+} \quad (\text{seconds}) \quad (1)$$

where ΔV_{2s} is the change in storage surface potential, C_t is the storage layer capacity (insulator surface to mesh capacity), and i^+ is the positive ion current landing at the whole negative insulator surface, which is assumed to be constant during viewing-duration. The current, i^+ , can be measured as a function of tube potentials, tube pressure, p , and viewing-beam current i_v .

For a particular tube ($\Delta V_{2s} = 0.5$ volts, $C_t = 2 \times 10^{-7} \text{ f}$ *, $i_v = 0.4$ ma, $p = 10^{-7}$ mm Hg, $i^+ = 5 \times 10^{-9}$ amp.):

$$T_v = \frac{(0.5)(2 \times 10^{-7})}{(5 \times 10^{-9})} = 20 \text{ sec for a halftone picture.} \quad (2)$$

It can be seen from Eq. (1) that long useful viewing durations require low ion current, high storage layer capacity, and a small slope of the control characteristic. Also, the tolerable ΔV_{2s} may be several times higher for black-and-white than for half-tone pictures. It should be noted that the relatively high storage layer capacity of $0.2 \mu\text{f}$ is important for obtaining a long viewing-duration. Thus, at present, viewing durations much greater than 10 seconds (without compensation for ion landing as described below) are obtained at the expense of writing speed, brightness, or resolution.

Viewing Duration As Affected by Tube Design

The obtaining of a sufficiently high vacuum has been accomplished by using a glass bulb which has a low diffu-

* $C_t = (kA/11.1 \text{ d}) 10^{-12} \text{ f}$ where k is the dielectric constant, A the storage grid area, and d the thickness of the storage layer. For $k = 4.4$, $A = 100 \text{ cm}^2$, and $d = 2 \times 10^{-4} \text{ cm}$, $C_t = 2 \times 10^{-7} \text{ f}$.

sion rate for atmospheric helium^{36,37} by proper processing, and by using effective low-pressure getter processes. For example, the trapping of residual gas molecules by ionization and acceleration towards a negative collector surface has been used. Such ionization was accomplished by an ionization gauge built into the tube,³⁸ or by using the viewing beam itself with other carefully outgassed tube elements (such as bulb coatings) as collectors to produce the ionization.

For a constant viewing current, the amount of positive ion current reaching the storage surface can be greatly reduced if the image amplifier collector grid is operated as an ion reflector, i.e., operated at a potential which is positive with respect to all the electrodes between it and the viewing gun cathode (Fig. 34). However, the remaining ions coming from the spaces between this collector grid and the phosphor screen still land on the negatively-charged storage layer surface or its backplate.

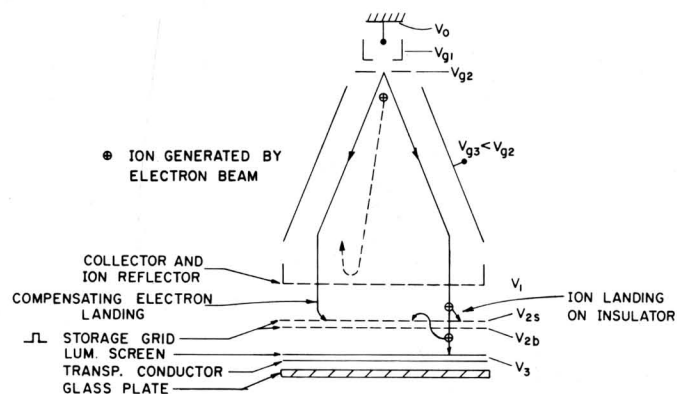


Fig. 34 - Positive ion landing at storage surface, and compensation by flood beam landing.

Increase of Viewing Duration by Pulsing or by a Separate Beam

In most applications such as radar and television, where one pattern is followed by another in a relatively rapid sequence, the viewing duration is sufficiently long for the operation cycle. However, for patterns which follow each other at a rate of less than 1 per minute, or at an arbitrary rate, a longer viewing duration is frequently desirable.

As outlined above, the only factor which limits viewing duration is the effect of positive ions landing at the surface of the storage target which drives negative-surface-potentials more positive, thus changing the picture background from black to gray.

In bistable operation, because of the holding action of the flood beam, ion landing is not detrimental; thus, continuous viewing is possible. In bipotential operation, ion landing is not detrimental as long as the black level

remains below the cut-off potential of the viewing current characteristic. In half-tone operation where the black level is equal to the cutoff level of the viewing current characteristic, an increase in viewing duration is frequently necessary. Two different methods have been developed: the compensation, and the bipotential-cathode holding method. Although the bipotential cycle can be achieved either with a separate erasing beam of different cathode voltage, or by pulsing the flood beam cathode or the storage grid, only the pulse methods are described here. It should be noted that the shifting cycle of the compensation method described below differs only slightly from the erasing process which is used in bipotential and half-tone operation. Fundamentally, for compensation, the storage surface elements in the area between the divide and a-b-c' (Fig. 29) receive an average current from the flood beam which is much smaller than the average erasing current. The erasing current depends on the erasing speed required; whereas, the average compensation current must be equal to the landing current of positive ions.

Compensation by Potential Shifting of The Storage Mesh. A rather crude method of partially compensating for the ion-landing is continually to shift the d-c potential of the storage mesh, thus temporarily shifting the storage surface to more negative values. The potential of the storage mesh may be manually adjusted by the operator to approximately compensate for the ion-landing by keeping the dark background constant. Although some extension of the viewing duration is possible by this method, the picture soon deteriorates because of the nonuniformity of the ion-landing.

Compensation With Pulsed Flood Beam. It is possible to compensate for the positive ions by an equal net current of viewing-beam electrons landing below the first crossover of the secondary emission curve. Since the ions are generated by the viewing-beam itself, they will land in a pattern which corresponds roughly to the current density of the viewing-beam. Therefore, the electron-landing will charge the storage grid negative in approximately the same

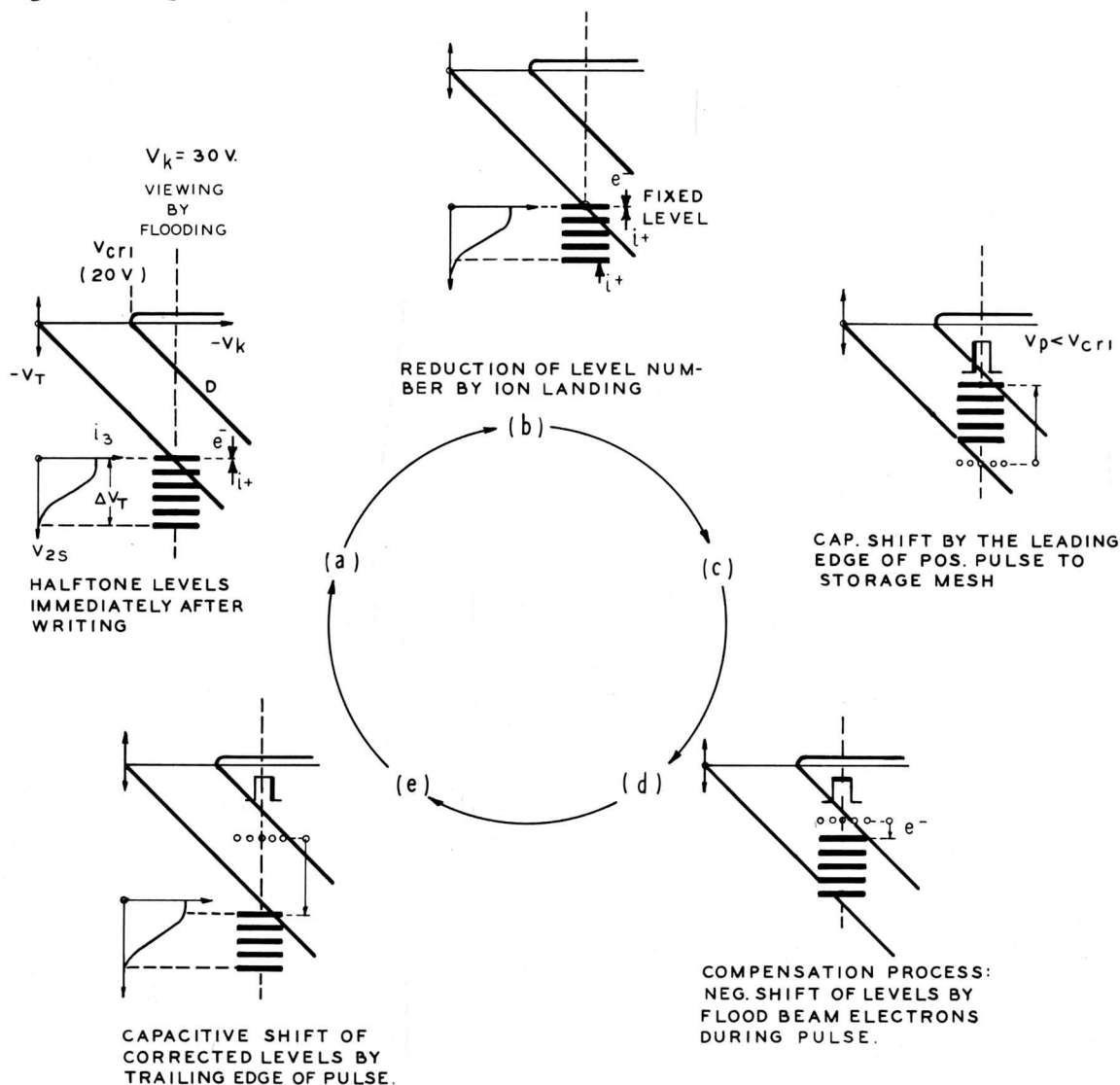


Fig. 35 - Increase of viewing duration by compensation with pulsed flood beam.

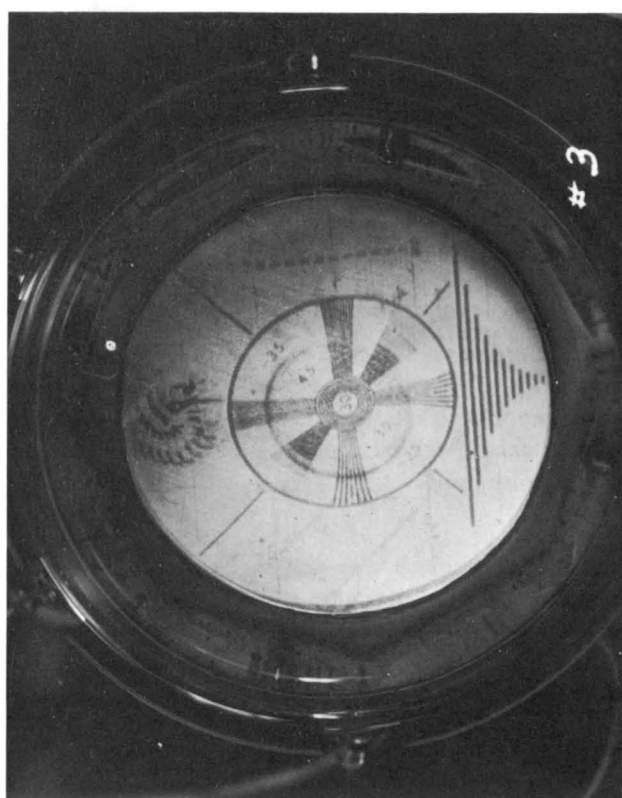
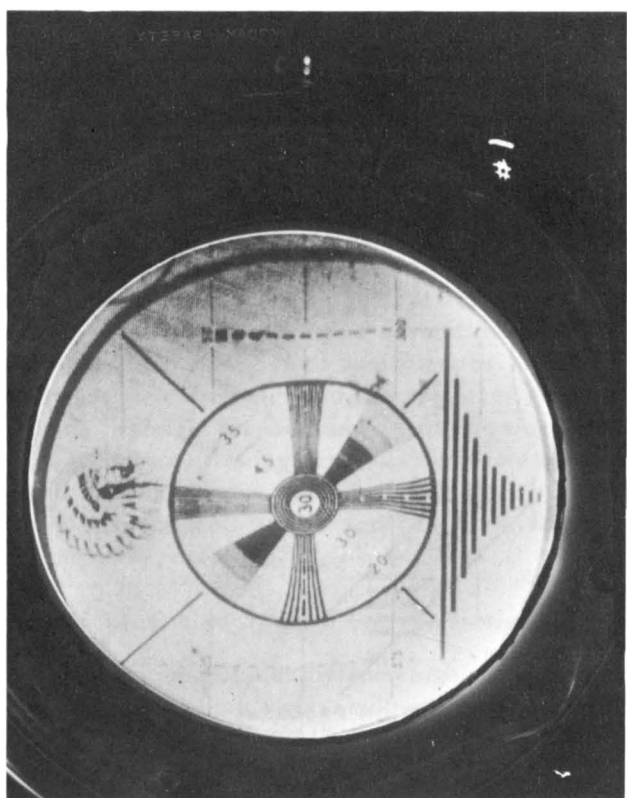
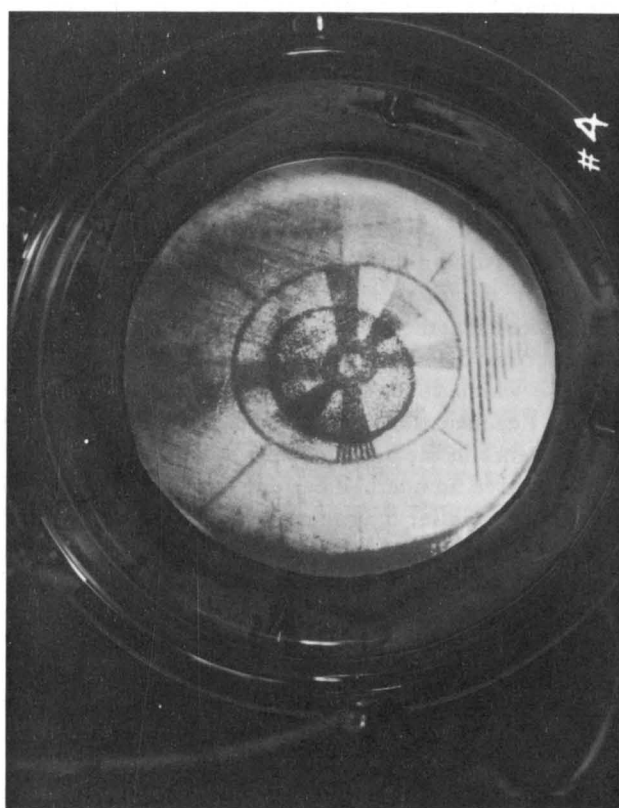
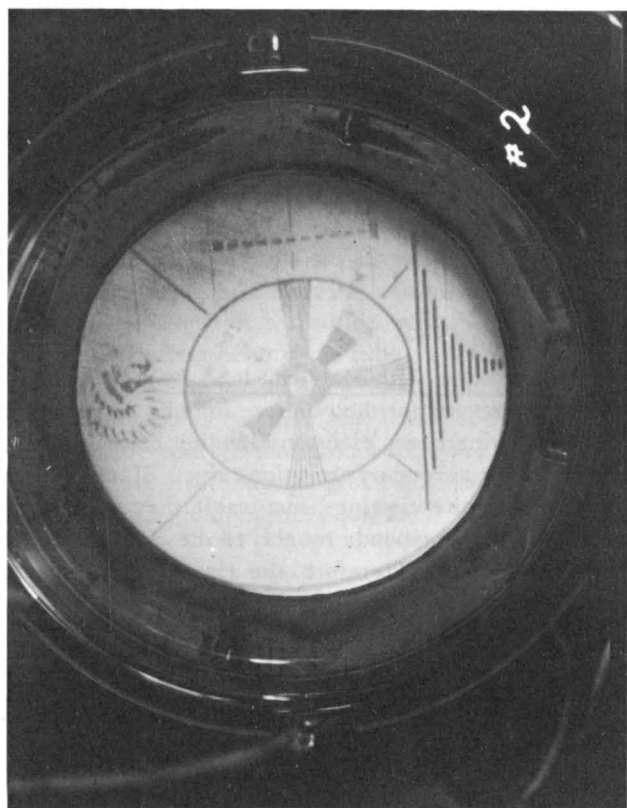


Fig. 36 — Illustration of the effect of methods for extending the viewing duration.

pattern that the positive ions have charged it positive. This landing may be achieved by pulsing the storage grid positive (or the viewing-gun cathode negative) at a repetition rate high enough to avoid flicker. In an experimental tube using microsecond pulses at a 60-per-second repetition rate, the viewing duration was extended by a factor of six (from 30 seconds to 3 minutes). In Fig. 35, the corresponding potential shifting cycle is given together with the viewing current characteristic. In this figure, the ion shift between two pulses is indicated by the loss of one of originally six half-tone levels. Actually, less than 1 percent of the contrast range, ΔV_T , is lost by ion-landing in the 1/60 sec between two of the microsecond pulses. As seen from Fig. 35, during the pulse the landing of electrons shifts the target areas negative by an amount equal to the positive shift of the ions between pulses. For this compensation, the pulse height is adjusted to less than V_{cr1} so that all half-tone levels remain below the potential divide during electron landing.

Fig. 36 shows the familiar monoscope test pattern. The first picture was taken immediately after writing. The second shows the deterioration by positive ions after 30 seconds storage. The third shows a similar stored half-tone picture with compensation by electron-landing after 3 minutes.

Bipotential Cathode Holding With Pulsed Flood Beam. Whereas with the compensation method all levels

are driven negative during pulsing by the flooding beam, in the bipotential-cathode holding method (Fig. 37) former black levels are driven negative and white levels positive during each pulse. Thus, the original potential range, ΔV_T , between white and black levels, which is reduced by positive ion-landing between pulses, may be not only restored during the pulse time but also substantially increased.

The potential of the positive pulses applied to the storage grid (or negative pulses to the viewing cathode) is chosen slightly higher than the first crossover potential ($2V_{cr1} > V_{pulse} > V_{cr1}$), so that target potentials close to white level are shifted above the potential divide but potentials close to black level are maintained below the divide (Fig. 37). During the pulse, viewing electrons will land with energies greater than first crossover at highlight storage surface areas, and with energies less than first crossover at dark storage surface areas. Thus, the more positive areas of the storage layer are driven towards a more positive potential, and the more negative storage layer areas are driven towards a more negative potential during the pulse. This pulse method, therefore, is distinct from the static-holding method proposed by Haeff³⁹ and the pulse holding method of Smith and Brown⁴⁰. The latter improves the contrast of a picture already held continuously in bistable operation by pulsing the holding (viewing) beam cathode negative so as to shift the negative black equilibrium potential still more negative.

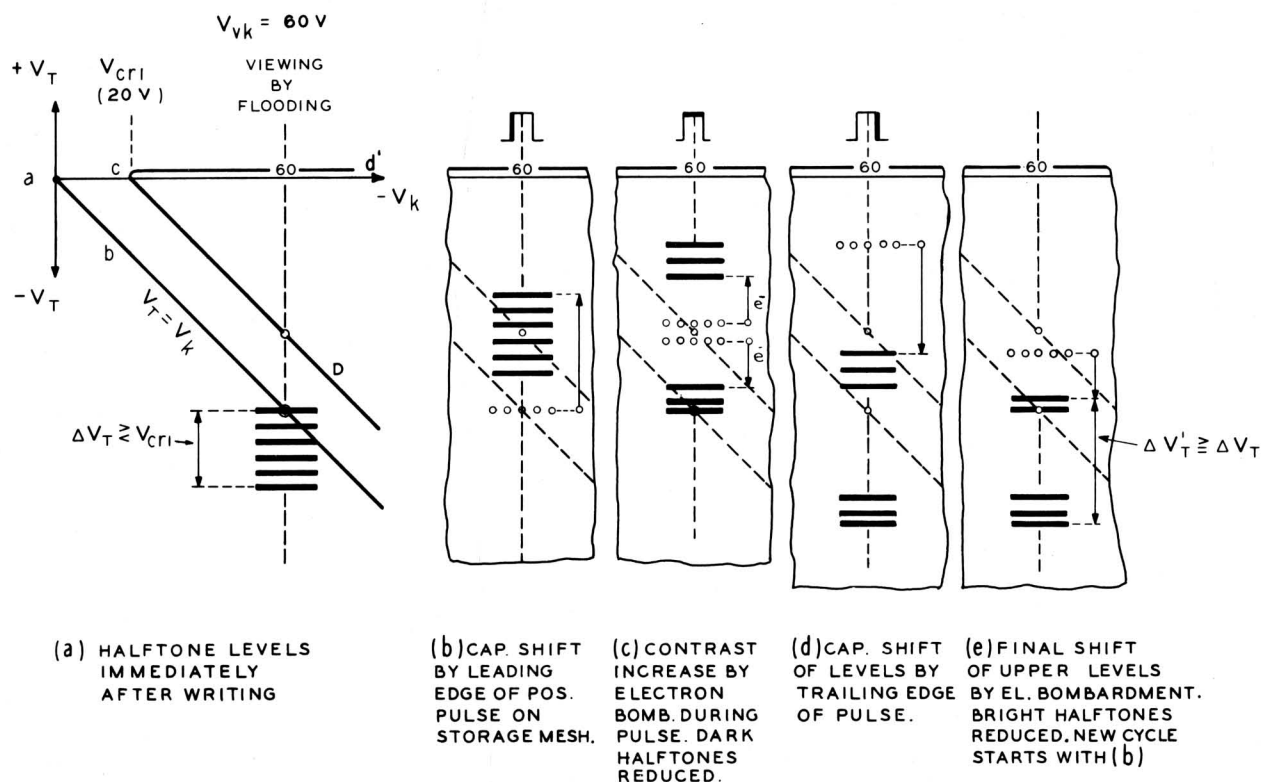
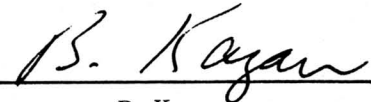


Fig. 37 - Increase of viewing duration by bipotential-cathode holding with pulsed flood beam.

Viewing Storage Tubes

Because the highlight levels are compressed during the back of the pulse (Fig. 37), this method does not appear suitable for preserving half-tones. In practice, with this method, a limited amount of half-tone can be stored. It was found that the compensation of a half-tone by flood-beam landing gave good stored pictures up to 3 minutes,

after which the compensated picture deteriorated. The "pulse-held" picture (Fig. 36 #4) soon lost much of its half-tone quality, but it could be held for hours. Starting with a black-and-white pattern, viewing durations as long as 27 hours have been observed with bipotential-cathode holding.



B. Kazan



M. Knoll

References

1. See, for example, H. W. Leverenz, INTRODUCTION TO THE LUMINESCENCE OF SOLIDS, John Wiley and Sons, New York, 1949.
2. See, for example, A. H. Rosenthal, "A System of Large-Screen Television Reception Based on Certain Electron Phenomena in Crystals", *Proc. IRE*, 28, 203, (May 1940); H. Kurzke and J. Rottgardt, "Über die Entfärbung von Alkalihalogenidkristalliten", *Ann. d. Phys.* Vol. 39, 619 (1941) and 41, 584 (1942).
3. L. Pensak, "The Graphechon -- A Picture Storage Tube", *RCA Review*, X, 59, (March 1949).
4. L. Pensak, "The Metrechon", A Half-Tone Picture Storage Tube", *RCA Review*, XV, 145, (June, 1954).
5. See, for example, M. Knoll, P. Rudnick, and H. Hook, "Viewing Storage Tube with Halftone Display", *RCA Review*, Vol. XIV, 492, (Dec. 1953).
6. Concerning the basic properties of such transmission control tubes, and the use of electron lens raster image amplifiers for them, see M. Knoll, "Electron Lens Raster Systems", in *Reports of the National Bureau of Standards Symposium on Electron Physics*, Nov. 5-7, (1951).
7. S. T. Smith and H. E. Brown, "Direct Viewing Memory Tube", *Proc. IRE*, 41, 1167 (Sept. 1953).
8. M. Knoll, and P. Rudnick, "Electron Lens Raster Viewing Storage Tubes", Washington Symposium on Electron Physics, NBS Circular No. 527, Nov. 5-7, 1951.
9. N. Knoll, H. O. Hook, and R. P. Stone, "Characteristics of a Transmission Control Viewing Storage Tube with Halftone Display", *Proc. IRE*, 42, 1496, (Oct. 1954).
10. H. O. Hook, M. Knoll, and R. P. Stone, "Viewing Storage Tubes For Large Displays", *RCA Review*, Vol. XVII, March, 1956.
11. *Iatron*, manufactured by Capehart - Farnsworth Corp., Fort Wayne, Indiana.
12. I. Langmuir, U. S. Patent 1,558,437.
13. H. Rothe and W. Kleen, GRUNDLAGEN UND KENNLINIEN DER ELEKTRONENROEHREN, Leipzig, Ger., pp. 297-298; see also H. A. Pidgeon, "Theory of Multi-Electrode Vacuum Tubes", *Bell Sys. Tech. Jour.*, Vol. 14, pp. 44 and 72, 1935.
14. M. Knoll, *Z. f. angewandte Physik* 6, 442 (1954).
15. For similar shapes of electron current distribution in electron spots produced with beams focused by an electric lens with spherical aberrations see M. Knoll, *Z. f. Physik* 15 (1934), p. 586; K. Kiels, and M. Knoll, *Techn. Physik* 16 (1935).
16. Analogous problems are discussed by J. L. H. Jonker, "The Control of Current Distribution in Electron Tubes", *Philips Res. Report* 1, 1945-46, p. 321 and 333.
17. H. Rothe and W. Kleen, GRUNDLAGEN UND KENNLINIEN DER ELEKTRONENROEHREN, Leipzig, 1948, p. 297.
18. See M. Knoll, F. Ollendorff, and R. Rompe, GASENTLADUNGSTABELLEN, p. 109, and H. Rothe and W. Kleen, l.c.p. 85.
19. M. P. Wilder, "Electrodes for Vacuum Tubes by Photogravure", *Proc. IRE*. 37 (Oct. 1949) 1182.
20. H. B. Law, "A Technique for the Making and Mounting of Fine Mesh Screens", *Rev. Sci. Instr.* 19 (Dec. 1948) 879.
21. H. B. Law, "A Three Gun Shadow Mask Color Kinescope", *Proc. IRE* 39 (Oct. 1951) 1192 and B. E. Barnes and R. D. Faulkner, same issue, p. 124.
22. For a description of these and the following processes mentioned, see M. Knoll and B. Kazan: STORAGE TUBES AND THEIR BASIC PRINCIPLES, N. Y., 1952, p. 22
23. H. B. Law, "Formation of Insulating Layers by The Thermal Decomposition of Ethyl Silicate", *Rev. Sci. Instr.* 20 (1949) p. 958.
24. See, e.g., F. H. Harris, "Progress on the NRL Halftone Memory Tube", *Panel on Electron Tubes, Symposium on Storage Tubes*, Washington, D.C., April 28, 1953.
25. M. Knoll, "Electron Lens Raster Systems", and M. Knoll and P. Rudnick, "Electron Lens Raster Viewing Storage Tube", *Rep. Nat. Bur. of Standards, Symp. on El. Physics*, Nov. 5, 1951.
26. R. C. Hergenrother and B. C. Gardner, "The Reading Storage Tube", *Proc. IRE* 38 (1950) p. 740.
27. S. T. Smith and H. E. Brown, "Direct View Memory Tube", *Proc. IRE* 41 (1953) p. 1167.
28. According to the well known "Electron Scanner" method (see M. Knoll, *Z.F. Techn. Physik* 16 (1935) p. 467, and C. E. Burnett, *RCA Review*, 2 (1938) p. 414).
29. See, for example, M. Knoll, O. Hachenberg and J. Randmer, *Z. F. Physik* 122 (1944) p. 150.

References (cont'd)

30. M. Knoll and R. Theile, *Z. F. Physik*, 113 (1939) p. 260. The auxiliary beam may be of the scanning or the spray type, and have velocities below the first or above the second crossover of the secondary emission curve.
31. For the superposition of surface and volume patterns in secondary emission pictures, see O. Hachenberg, and J. Randmer, *Z. F. Physik.*, 122 (1944) p. 137.
32. STORAGE TUBES AND THEIR BASIC PRINCIPLES, M. Knoll and B. Kazan, John Wiley and Sons, Inc., New York, N.Y. 1952. For potential shifts typical of different storage and television camera tubes see *Archiv der el Vbertragung*, Vol. 4 (1950) p. 238.
33. Detailed discussion of these types of erasure is given by M. Knoll, H. Hook, and R. Stone, *Proc. IRE* 1954, p. 1503.
34. A. V. Haeff, *Electronics* 20 (Sept. 1947) p. 80. The adaptation of this mechanism for grid control reading is described by S. T. Smith and H. E. Brown in *Proc. IRE* 41 (Sept. 1953) p. 1167.
35. For attempts to use this mechanism for halftone operation also, see F. H. Harris: "Progress on the NRL halftone memory tube". *Abstr. Symp. on Storage Tubes* (April 28, 1953), Panel of Electron Tubes, Washington, D.C.
36. For details, see R. P. Stone, "Some Problems in the Design of a Direct View Storage Tube; Techniques for Maintaining High Vacua", *N.Y. Nat'l. Conf. Elec. Tube Teche.*, Oct. 15, 1953.
37. See also Lord Rayleigh, *Proc. Roy. Soc.*, London, Eng., Vol. 156, p. 350 August, 1936; D. Alpert and R. S. Burwitz, *Jour. Appl. Phys.*, Vol. 25, 202: February, 1954.
38. See G. Krawinkel and T. F. Adams, *Fiat Rep.* 1021, PB-78273; April, 1947. And D. Alpert, *Jour. Appl. Phys.*, Vol. 24, p. 860; July, 1953. Also H. Schwarz *Z. fur Phys.*, Vol. 122, p. 437; 1944.
39. A. V. Haeff: "A Memory Tube", *Electronics*, Vol. 20 (Sept. 1947) p. 80.
40. S. T. Smith and H. E. Brown: "Direct Viewing Memory Tube", *Proc. IRE.*, Vol. 41, (Sept. 1953) p. 1167.

